AD-A046 629 EARTH SATELLITE CORP WASHINGTON D C F/G 4/2
A PRELIMINARY STUDY OF THE APPLICABILITY OF NIMBUS 6 ESMR TO SE--ETC(U)
SEP 76 R R SABATINI, L J HEITKEMPER N00228-75-C-2269
UNCLASSIFIED NEPRF-TR-6-76(ESC) NL

| OF |
AD
A046629

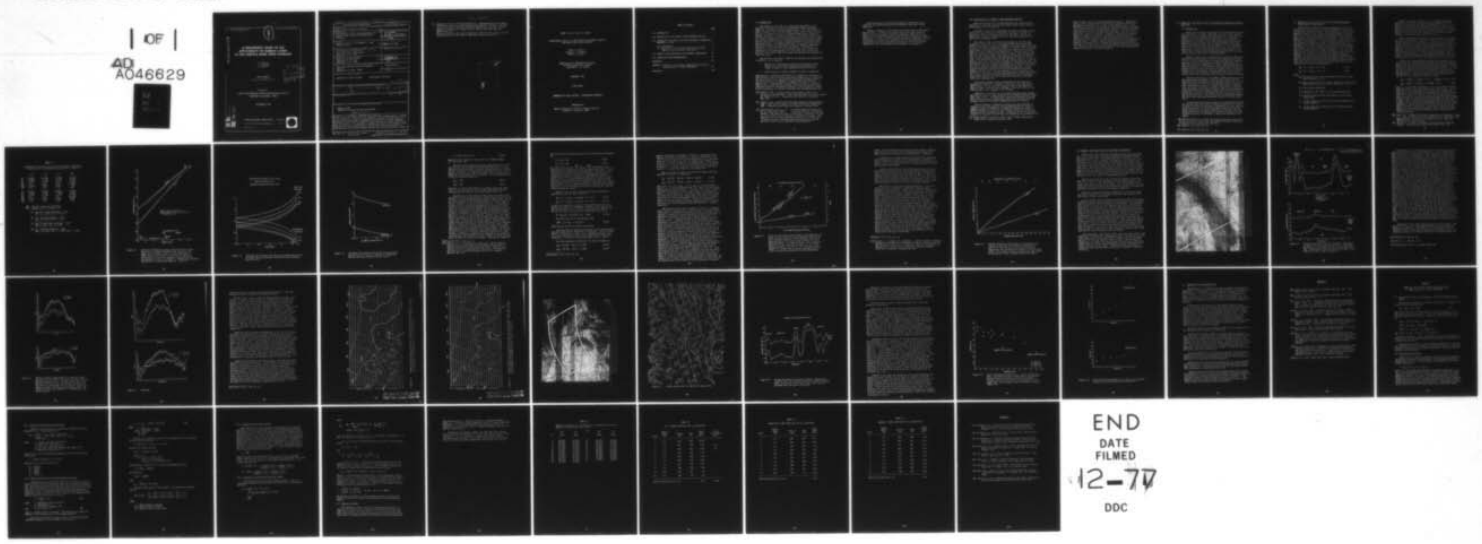

END
DATE
FILMED
12-77
DDC

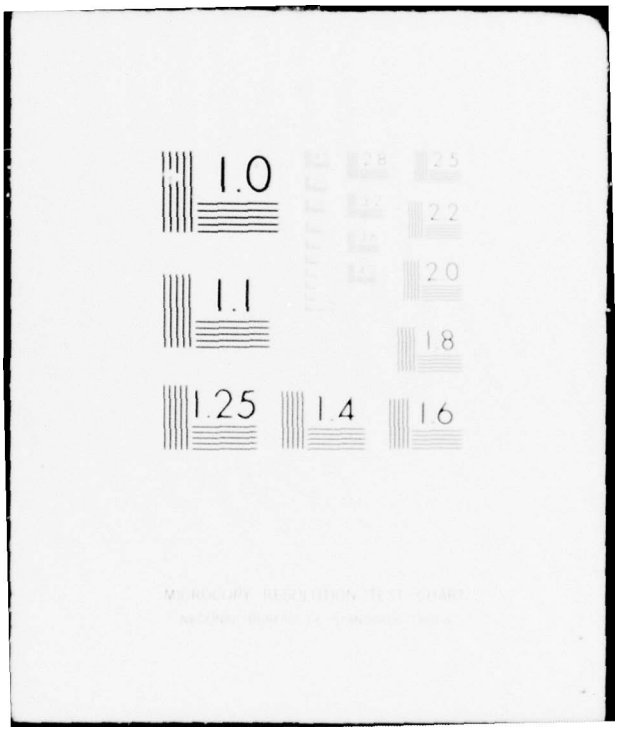
1.0
1.1
1.25
1.4
1.6
2.0
2.2
2.5
1.8

NEPRF Technical Report 6-76 (ESC)

4

B. S

A PRELIMINARY STUDY OF THE APPLICABILITY OF NIMBUS 6 ESMR TO SEA-SURFACE WIND SPEED ESTIMATES

R. R. SABATINI
L. J. HEITKEMPER
D. L. HLAVKA

FINAL REPORT

Contract No. N00228-75-C-2269

Prepared for:

NAVAL ENVIRONMENTAL PREDICTION RESEARCH FACILITY
MONTEREY, CALIFORNIA 93940

SEPTEMBER 1976

EARTH SATELLITE CORPORATION *(EarthSat)*

7222 47th St. (Chevy Chase), Washington, D. C. 20015

(301) 652-7130

SECURITY CLASSIFICATION OF THIS PAGE (When Data Entered)

(19) TR-6-76 (ESC)

REPORT DOCUMENTATION PAGE	READ INSTRUCTIONS BEFORE COMPLETING FORM
1. REPORT NUMBER: NEPRF Technical Report 6-76 (ESC)	2. GOVT ACCESSION NO. / 3. RECIPIENT'S CATALOG NUMBER
4. TITLE (and Subtitle): A Preliminary Study of the Applicability of Nimbus 6 ESMR to Sea-surface Wind Speed Estimates.	5. TYPE OF REPORT & PERIOD COVERED: Final Report, May 1975 – Sept. 1976
	6. PERFORMING ORG. REPORT NUMBER: C-1838
7. AUTHOR(s): Sabatini, Romeo, R.; Heitkemper, L.; and Hlavka, Dennis L.	8. CONTRACT OR GRANT NUMBER(s): N00228-75-C-2269
9. PERFORMING ORGANIZATION NAME AND ADDRESS: Earth Satellite Corporation, 7222 47th Street (Chevy Chase), Washington, D.C. 20015 (12) 54 p.	10. PROGRAM ELEMENT, PROJECT, TASK AREA & WORK UNIT NUMBERS
11. CONTROLLING OFFICE NAME AND ADDRESS: Naval Air Systems Command, Department of the Navy, Washington, D.C. 20361	12. REPORT DATE: September 1976
	13. NUMBER OF PAGES: 45
14. MONITORING AGENCY NAME & ADDRESS (if different from Controlling Office): Naval Environmental Prediction Research Facility, Monterey, California 93940	15. SECURITY CLASS. (of this report): Unclassified
	15a. DECLASSIFICATION/DOWNGRADING SCHEDULE

16. DISTRIBUTION STATEMENT (of this Report)

Approved for Public Release Distribution Unlimited

DDC

17. DISTRIBUTION STATEMENT (of the abstract entered in Block 20, if different from Report)

Romeo R./Sabatini, Lawrence J./Heitkemper, Dennis L./Hlavka

DDC RECEIVED NOV 16 1977 F

18. SUPPLEMENTARY NOTES

19. KEY WORDS (Continue on reverse side if necessary and identify by block number)

Nimbus 6 ESMR
Satellite Microwave for Sea-surface Winds
brightness temperatures

20. ABSTRACT (Continue on reverse side if necessary and identify by block number)

The utility of the Nimbus 6 ESMR for sea-surface wind determination is explored in this study by: 1) analysis of wind equations derived from theoretical calculations of T_B above model atmospheres and assumptions of linear increases in sea-surface emissivities with wind, 2) actual analysis of Nimbus 6 ESMR T_B in areas of known wind. Unfortunately a calibration problem in the Nimbus 6 ESMR prevented quantitative comparisons of T_B and wind, and the derivation of a sound empirical relationship between wind and sea-surface emissivities needed to

DD FORM 1 JAN 73 1473 EDITION OF 1 NOV 65 IS OBSOLETE S/N 0102-014-6601

Unclassified 407 476

SECURITY CLASSIFICATION OF THIS PAGE (When Data Entered)

brightness temperatures

20. estimate winds from satellite-measured T_B's. Notwithstanding the erroneous calibration, analyses of ESMR T_B maps do show definite increases in horizontally and vertically polarized brightness temperatures with wind. Such increases are dramatically brought out in a Mistral occurrence over the Mediterranean Sea.
An error analysis on derived wind equations establishes the accuracy of wind speed determination from Nimbus 6 ESMR under various conditions.

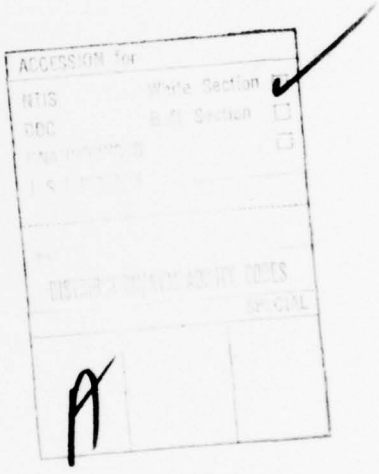

NEPRF Technical Report 6-76(ESC)

A PRELIMINARY STUDY OF THE APPLICABILITY OF NIMBUS 6 ESMR TO SEA-SURFACE WIND SPEED ESTIMATES

Romeo R. Sabatini
Lawrence J. Heitkemper
Dennis L. Hlavka

EARTH SATELLITE CORPORATION (EarthSat)
7222 47th Street (Chevy Chase)
Washington, D.C. 20015

September 1976

Final Report

Prepared For:

Naval Environmental Prediction Research Facility
Monterey, California 93940

TABLE OF CONTENTS

1.0 INTRODUCTION

The purpose of this study is a preliminary assessment of the utility of the Nimbus 6 Electrically Scanning Microwave Radiometer (ESMR) for sea-surface wind speed determination. The 37 GHz Nimbus 6 ESMR, successor to the 19.35 GHz Nimbus 5 ESMR, differs from the latter not only in frequency but also in scanning geometry and polarization. Previous studies [1, 2] proved the utility of the Nimbus 5 ESMR to sea-surface wind determination, but also pointed out the deleterious effects of a cloudy atmosphere and of the not-well-defined relationship between wind and wave spectrum on the ultimate estimation of wind from brightness temperatures. The Nimbus 6 ESMR with its dual polarization would partially compensate for atmospheric effects by providing additional information in the vertically polarized channel. Nevertheless, in precipitation areas and in areas of liquid clouds the uncertainties introduced by the atmosphere are still too large, thus limiting the ability of the Nimbus 6 ESMR for accurate sea-surface wind estimation to cloud-free areas.

The utility of the Nimbus 6 ESMR for sea-surface wind determination is explored in this study by:

1. Analysis of wind equations derived from theoretical calculations of T_B above model atmospheres and assumptions of linear increases in sea-surface emissivities with wind.

2. Actual analysis of Nimbus 6 ESMR T_B in areas of known wind.

Unfortunately a calibration problem [3] still present in the Nimbus 6 ESMR (September 1976) prevented quantitative comparisons of T_B and wind, and the derivation of a sound empirical relationship between wind and sea-surface emissivities needed to estimate winds from satellite-measured TB's. Notwithstanding the erroneous calibration, analyses of ESMR T_B maps do show definite increases in horizontally and vertically polarized brightness temperatures with wind. Such increases are dramatically brought out in a Mistral occurrence over the Mediterranean Sea.

---

[1] Sabatini, R.R., "The Application of the Nimbus 5 ESMR to Sea-Surface Wind Determination." EPRF Technical Report 5-74 (ESC) Contract No. N66314-73-C-1572. Prepared by Earth Satellite Corporation, May, 1974.

[2] Sabatini, R.R., "Sea-Surface Wind Speed Estimates from the Nimbus 5 ESMR." EPRF Technical Report 3-75 (ESC) Contract No. N66856-4120-5501. Prepared by Earth Satellite Corporation, February 1975.

[3] Communications with Dr. T. Wilheit the NASA ESMR Experimenter and Dr. A. Chang also of NASA confirmed our suspicions of a calibration problem. ESMR data are presently available in calibration versions 11, 12, 13, and 14 all of which are incorrectly calibrated. ESMR data were first received from NASA in versions 11, 12 and later in version 14 which, although gridded more accurately than the previous versions, still contained a calibration error.

An error analysis on derived wind equations establishes the accuracy of wind speed determination from Nimbus 6 ESMR under various conditions.

Section 2 presents a brief description of the Nimbus 6 ESMR experiment and data. In Section 3 we discuss the surface and atmospheric effects on to the microwave brightness temperatures measured by the Nimbus 6 ESMR, and develop equations defining the relationship between wind and T_B. Section 4 presents analyses of Nimbus 6 ESMR data. Section 5 concludes the report with a summary of results and recommendations. The equations and model atmospheres employed to calculate brightness temperatures above the atmosphere are presented in the Appendix.

2.0 DESCRIPTION OF THE NIMBUS 6 ESMR EXPERIMENT AND DATA

Only the essentials will be presented here; for a more detailed description of the ESMR experiment the reader should consult Section 5 of the Nimbus 6 User's Guide [4].

The ESMR is one of eight experiments carried by the Nimbus 6 spacecraft which was launched in a near-polar, circular (1,100 km), sun-synchronous (noon to midnight) orbit on 12 June 1975. Most of the experiments, including the ESMR, are still functioning properly as of this writing (September 1976).

The Nimbus 6 ESMR is sensitive to radiation in a 250 MHz band centered at 37 GHz (0.81 cm). The Nimbus 6 ESMR measures both horizontally and vertically polarized components of the microwave radiation by using two separate radiometer channels. The antenna beam of the ESMR scans ahead of the spacecraft along a conical surface with a constant angle of 45° with respect to the antenna axis. The beam scans in azimuth ±35° about the forward direction in 71 steps, such that beam position 1 is 35° azimuth angle to the right of the spacecraft, beam position 36 views straight ahead, and beam position 71 views 35° to the left. The instantaneous field-of-view (half-power contours) is approximately an oval, 20 x 40 km, nearly constant in size along the scan. The scan geometry and the tipping of the antenna 5° forward of the vertical axis of the spacecraft permits the antenna beam to intersect the earth at a nearly constant incidence angle throughout the scan. For the expected spacecraft pitch bias of +0.6° the incidence angle varies between an angle of 50.8° for scan positions 1 and 71, and 49.6° for position 36. The nearly constant incidence angle eliminates the effects of a varying nadir angle on sea-surface emissivity and on atmospheric optical path lengths, thus facilitating both qualitative and quantitative data interpretation.

The scanning geometry nearly compensates for the distortions introduced by the earth's curvature. The width of the image area is approximately 1,270 km, causing substantial gaps in the equatorial regions between successive orbit coverages. These gaps decrease away from the equator and disappear at 60° latitude.

ESMR data are available to users from the National Space Science Data Center (NSSDC) in image format and on Calibrated Brightness Temperature Tapes (CBTT). The ESMR pictorial data and the Nimbus 6 catalogs [5] serve the purpose of determining coverage and selecting areas for in-depth analysis of brightness temperature values on the CBTT.

All our brightness temperature analyses have been performed on computer printout maps obtained from the NASA-provided CBT tapes. A computer program in FORTRAN and in ASSEMBLER languages for the IBM 360/168 computer was written to read the CBTT and to map out the calibrated brightness temperatures (CBT). Depending upon the instructions inserted in a control card, CBT data to be mapped can be selected on the

[4] Nimbus Project, "The Nimbus 6 User's Guide," NASA, Goddard Space Flight Center, Greenbelt, Maryland, 1975.

basis of time interval or latitude-longitude intervals. Additionally, one can choose to map either the vertical or horizontal polarization brightness temperatures (T_{Bv} or T_{Bh}) or the difference ($T_{Bv} - T_{Bh}$). The CBT maps contain all of the original unaveraged values of T_B mapped at a nearly one-to-one ratio between the vertical (along sub-satellite track) and the horizontal (cross-track) distances. The map is at an approximate scale of 1:2,200,000. Gridding of the map is achieved by means of a rubber-grid overlay. The overlay, coupled with satellite subpoint information on the CBTT and printed out on the CBT maps, greatly facilitates gridding to nearly the accuracy of the resolution of the ESMR system. Landmarks such as coastlines are used to correctly position the overlay grids. Although latitude-longitude information is available on the CBTT for every 15th beam position starting at position six, these were often found to have errors of more than one degree and therefore not usable for accurate gridding.

3.0 ATMOSPHERIC AND SURFACE EFFECTS ON BRIGHTNESS TEMPERATURES MEASURED AT 37 GHz

3.1 Introduction

Theory and experiments have shown that the microwave emissivity, and therefore the resultant temperature of a sea-surface, depends strongly on the sea roughness and foam and spray. Since these are related to the wind velocity near the surface, sea brightness temperatures T_B measured from a satellite can be a measure of the sea-surface wind velocity. The relationship between brightness temperature and sea-surface wind is complicated by factors which can be arbitrarily divided into two groups: (1) those atmospheric factors that influence the transfer of microwave energy from the sea-surface to the satellite sensor; and (2) those boundary layer factors that influence the relationship between wind and sea state, or the effective emissivity* of the sea-surface.

Previous studies [6, 7] indicated that the Nimbus 5 ESMR could estimate sea-surface winds to a five- to six-knots probable error (7.5 to 9 knots standard error) in clear areas and fully developed open seas, given a climatological estimate of atmospheric water vapor and sea-surface temperatures. These studies pointed out that the main difficulty is the definition of an accurate relationship between wind and surface emissivity, the quantity that is actually derived from T_B measurements, and also ruled out the use of Nimbus 5 ESMR T_B for wind estimates in rainy and cloudy areas (except cirrus) unless the cloud liquid water could be accurately estimated.

The two polarizations of the Nimbus 6 ESMR essentially provide two simultaneous measurements of the T_B, which under clear sky conditions permit estimates of the horizontal and vertical polarization sea-surface emissivities, which are both related to surface wind. Nevertheless, there still remains the problem of interpreting the derived emissivities in terms of wind; even in perfectly clear atmospheres the ultimate accuracy of the wind estimate relies on how well the sea wave spectrum, foam, and spray (all of which control emissivities) can be equated to wind. As we shall show in the following sections, even with the two T_B measurements presence of liquid clouds may cause unacceptable errors in the wind estimates.

In the following sections we shall derive simplified equations for the horizontal and vertical brightness temperatures at 37 GHz in terms of surface and atmospheric parameters, use these equations and an assumption of a linear relationship between wind and sea-surface emissivities to derive equations for the wind, and ultimately speculate on the magnitude of the errors caused to the wind estimates by errors in estimates of surface and atmospheric parameters.

*By effective emissivity is meant the integrated average emissivity of an area at least as large as the resolution of the sensor, containing an ensemble of waves, white caps, and spray.

[6] Sabatini, R.R., 1974, Op. Cit.

[7] Sabatini, R.R., 1975, Op. Cit.

3.2 Derivation of Sea-Surface Emissivities and Wind Equations from Brightness Temperatures

The brightness temperature above the atmosphere can be calculated for given atmospheric and surface conditions by means of the radiative transfer equation. In our approach, called the thin-atmosphere approximation and detailed in the Appendix, the atmosphere is divided into many layers each having an average temperature, water content, and absorption coefficient. The radiation emerging from the ocean surface is transferred layer-to-layer up to the top of the atmosphere. In order to derive a simple expression for brightness temperature in terms of surface emissivity and atmospheric and surface parameters, we solved the radiative transfer equation for clear and cloudy (non-precipitating) atmospheres, with various sea-surface temperatures and emissivities. We then fitted the results with first order polynominals. The resulting equations are simpler to handle than the transfer equation and are amenable to error analyses. Two sets of equations have been derived: one set for the horizontally polarized brightness temperatures for which the emissivities were made to vary from 0.30 to 0.60, and another for the vertical polarization brightness temperatures for which the emissivities were varied from 0.60 to 0.75. The equations are of the following form:

$$T_{Bh} = k_o + k_1 E_h T_S + k_2 V + k_3 C \qquad (3.1)$$

$$T_{Bv} = k_4 + k_5 E_v T_S + k_6 V + k_7 C \qquad (3.2)$$

where

T_{Bv} and T_{Bh} are vertical and horizontal polarization brightness temperatures (°K);

E_v and E_h are vertical and horizontal polarization sea-surface emissivities ($0.30 \leq E_h \leq 0.60$), ($0.60 \leq E_v \leq 0.75$)

T_S is sea-surface temperature

V is atmospheric water vapor in cm of precipitable water

C is non-precipitating cloud liquid water in cm of precipitable water

k_o - k_3 are regression coefficients for the horizontal polarization equation

k_4 - k_7 are regression coefficients for the vertical polarization equation

Table 3-1 presents values of k_o - k_7, multiple correlation coefficients Mcc, and the standard error of estimate SEE for a variety of atmospheres described in the Appendix. Figure 3.1 is a plot of how the brightness temperatures vary for the given conditions as a function of emissivity calculated with our thin atmosphere assumption, and by means of regression equations 3.1 and 3.2. The plot gives an idea of the goodness of fit of the regression equations to thin atmosphere calculations of T_B.

Given the brightness temperatures and estimates of water vapor and cloud liquid content, equations 3.1 and 3.2 can be solved for the sea-surface emissivities (E_h, E_v). The emissivities in turn can be translated to a sea-surface wind by an appropriate empirical equation derived from Nimbus 6 ESMR. Unfortunately, the inadequately calibrated ESMR data did not permit us to derive reliable equations for the sea-surface emissivities (both horizontal and vertical polarization) as a function of observed winds. However, in our subsequent analyses, for the sake of estimating range of errors in the derived wind we shall assume linear emissivity versus wind equations derived from 37 GHz observations from an airplane.

The vertical and horizontal polarization sea-surface emissivities are not only determined by the waves, foam, and spray produced by the wind, but also by the zenith angle, and the water temperatures and salinity which control the dielectric constants. Figures 3-2 and 3-3, derived from calculations presented by Paris [8], show the sea-surface emissivities at 37 GHz for calm conditions and average salinity of 32.72 o/oo as a function of zenith angle and sea temperature. From these graphs we can approximate the emissivities for calm conditions at zenith = 50° by:

$$E_{ho} = 1.02059 - 0.162208 \times 10^{-2} T_S - 0.248206 \times 10^{-5} T_S^2 \quad (3.3)$$

$$E_{vo} = 5.4048 - 0.032738 T_S + 0.474646 \times 10^{-4} T_S^2 \quad (3.4)$$

where T_S is sea-surface temperature in °K. The creation of waves, foam, and spray by the wind increases these emissivities. At low wind speeds before any foam forms, surface waves of dimensions comparable to the wavelength of observations are primarily responsible for the emissivity changes. As the wind speed increases so does the roughness, but most importantly so does the foam coverage. Graphical plots of observations of foam coverage with wind [9] show a large scatter, indicating that many other factors affect foam coverage. These include the duration and fetch of the wind, water temperature, thermal stability (difference in water and air temperature), salinity, and variations in the surface tension of the water due to the occurrence of organic films. From all available observations of wind and foam coverage, Stogryn [9] derives the following equation:

[8] Paris, J.F., "Transfer of Thermal Microwave in the Atmosphere." Vols. 1, 2. Dept. of Meteorology, Texas A&M University. Prepared for NASA NGR-44-001-098, Office of Naval Research, Nour 2119 (04), and DOD Project No. 5013, May, 1971.

[9] Stogryn, A., "A Study of Radiometric Emission from a Rough Sea-Surface." NASA Contractor Report NASA CR-2088, July, 1972.

TABLE 3.1

Regression Coefficients for Estimating Brightness Temperatures at the Top of the Atmosphere with Equations 3.1 and 3.2

	(1)	(2)	(3)	(4)
k_0	29.4908	45.7560	47.4933	73.9178
k_1	0.8708	0.7392	0.7341	0.5704
k_2	9.8574	9.2946	9.2142	7.0457
k_3	0.0	0.0	0.0	624.654
MCC	0.9999	0.996	0.996	.992
SEE	0.33	1.80	2.12	2.69
k_4	32.6313	58.5909	60.8529	92.6543
k_5	0.8642	0.7407	0.7383	0.5755
k_6	5.2705	4.7083	4.7270	4.0150
k_7	0.0	0.0	0.0	351.633
MCC	0.999	0.995	0.995	0.995
SEE	0.713	1.82	2.01	1.74

MCC - multiple correlation coefficient
SEE - standard error of estimate (°K)

(1) Sub Arctic summer atmosphere - clear
$273 \leq T_s \leq 283$; $0.20 \leq V \leq 0.80$

(2) U.S. standard atmosphere - clear
$280 \leq T_s \leq 295$; $1.00 \leq V \leq 4.60$

(3) Mid-latitude summer atmosphere - clear
$290 \leq T_s$ 300; $1.50 \leq V \leq 5.50$

(4) U.S. standard atmosphere - cloudy
$280 \leq T_s \leq 295$; $1.00 \leq V \leq 4.60$; $0.02 \leq C \leq 0.06$

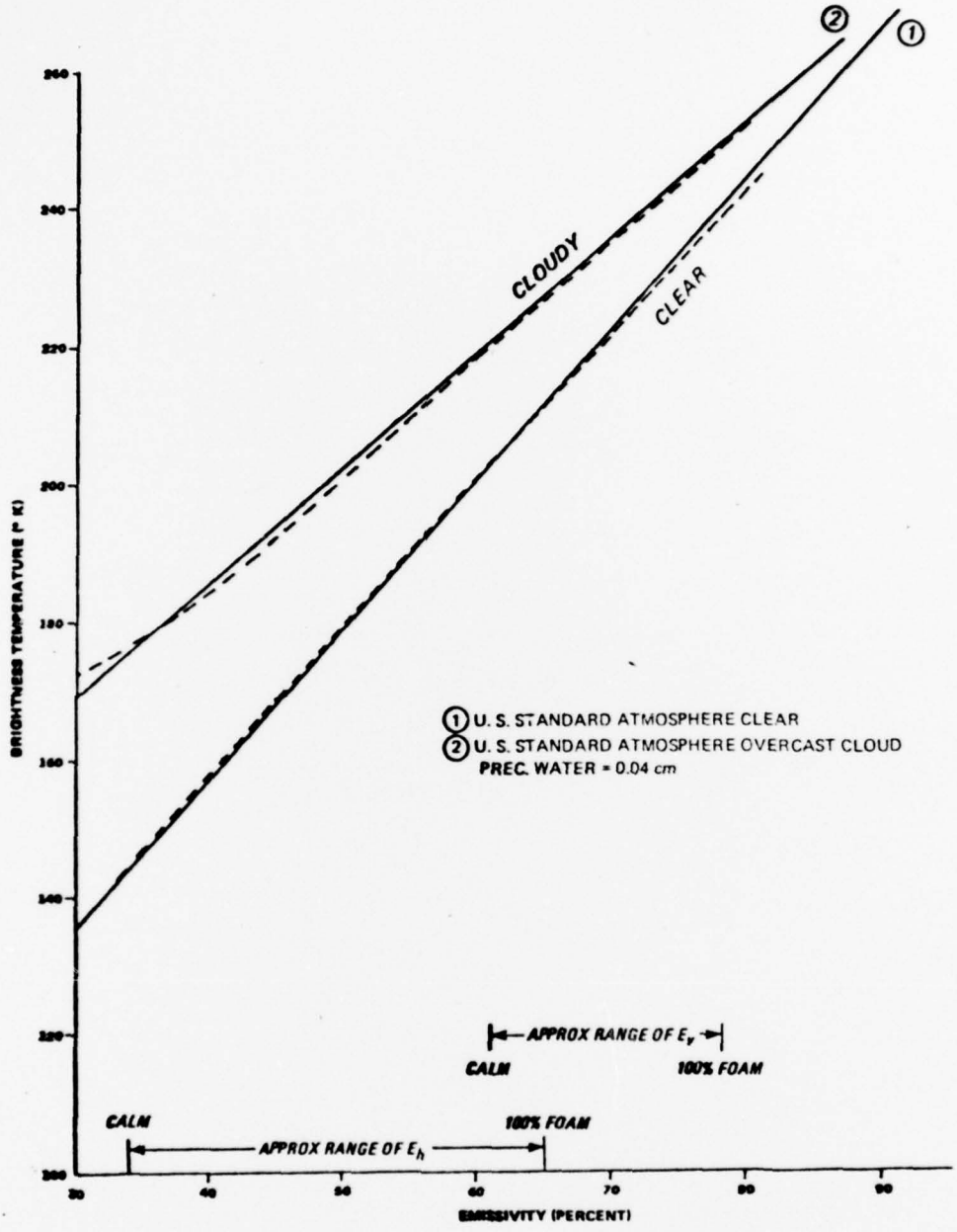

Figure 3-1 Brightness temperatures versus surface emissivity at the top of a U.S. Standard Atmosphere with clear sky, 100% clouds (0.04 cm precip. water), surface temperature of 290°K, and 50° zenith angle. Full lines are results of calculations with the thin atmosphere approximation and ten atmospheric layers (see Appendix). Dashed lines represent calculations with regression equations 3.1 and 3.2.

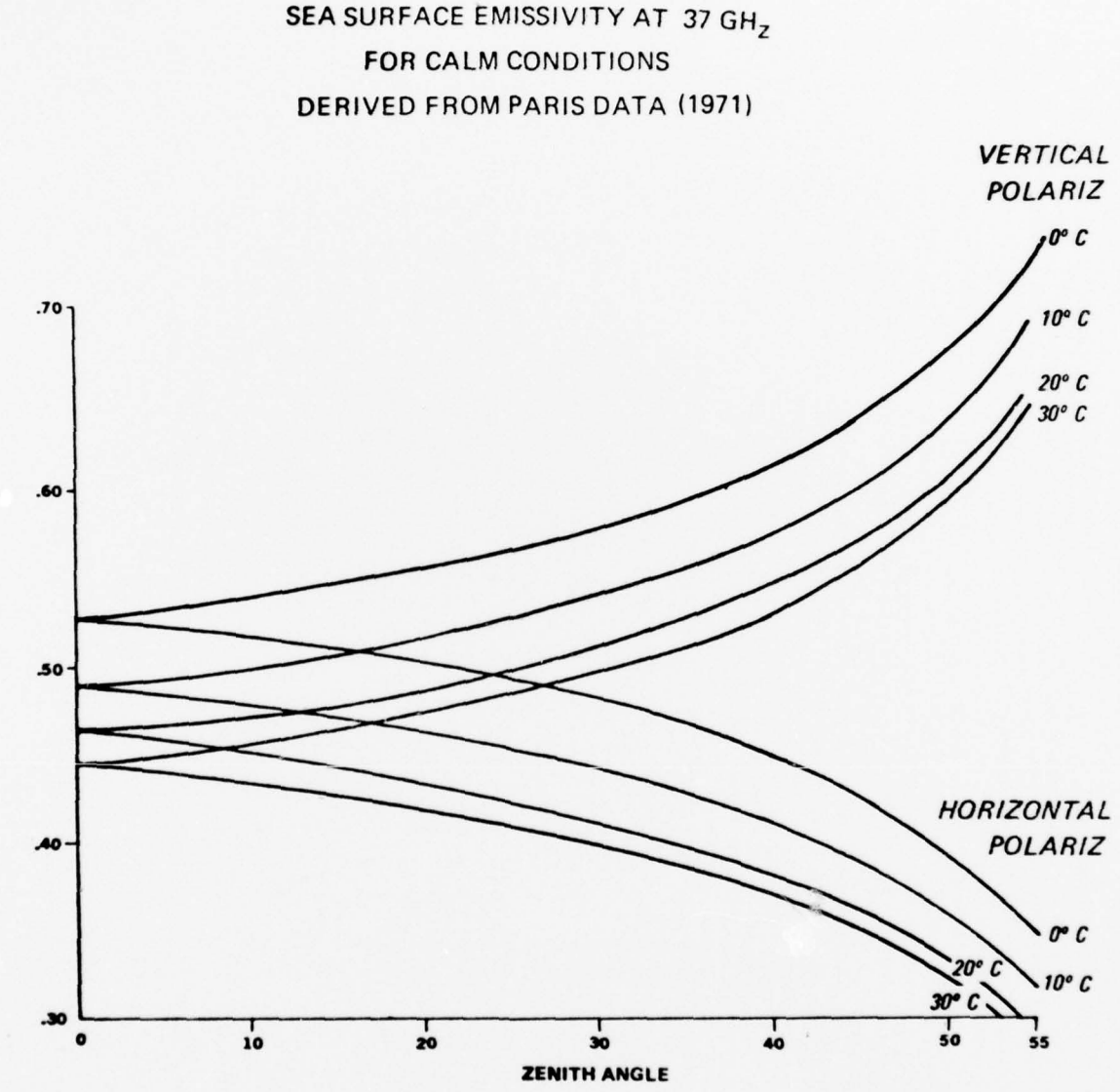

Figure 3-2 Horizontal and vertical polarization sea-surface emissivities at 37 GHz for calm conditions, derived from data presented by Paris (1971).

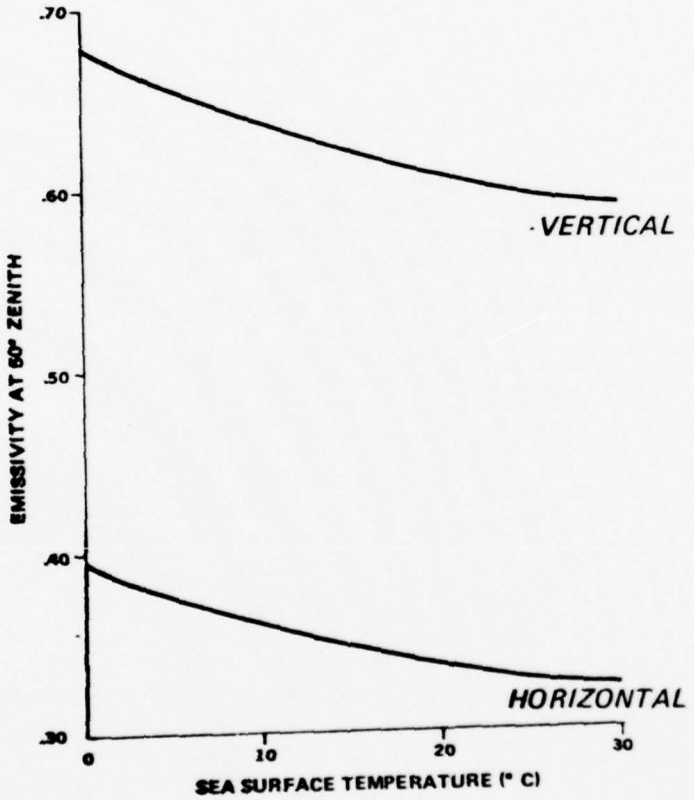

Figure 3-3 Horizontal and vertical polarization calm sea-surface emissivities at 37 GHz as a function of temperature, derived from data presented by Paris (1971).

$$F = 7.751 \times 10^{-4} W^{3.231} \quad (3.5)$$

where W is wind velocity in m/sec, and F is % foam coverage (F = 100 for W = 38)

The theoretical determination of microwave emissivity of foam also presents complex modeling problems that can best be circumvented by deriving empirical equations from observations. Stogryn [9] has synthesized all known data on foam emissivity into a set of empirical equations that express foam emissivity as a function of temperature, wavelength, and zenith angle. At 50° zenith angle and 37 GHz his equations reduce to:

$$E_h T_s = 190 \quad (3.6)$$

$$E_v T_s = 228 \quad (3.7)$$

Equations 3.3 and 3.6 show that at T_s = 293°K, E_h can vary from 0.33 for calm conditions to 0.65 for 100% foam cover; similarly from equations 3.4 and 3.7, E_v can vary from 0.61 to 0.78.

Considering only the effects of foam cover on the emissivity, equation 3.5 tells us that emissivity should increase slowly at low to medium speed winds and then much faster at higher winds. But as the wind increases, at low to medium speeds ($\leq$ 15 m/sec) there is also an increase to the emissivity due to waves. The combination of waves and foam may well be responsible for the nearly linear effect of wind to brightness temperature observed with 19.35 GHz satellite microwave data by Sabatini [10] in the Mediterranean and the Gulf of Tehuantepec (off Mexico), and observed with airborne microwave radiometers at various frequencies (including 37 GHz) by Webster et al. [11] in the Bering Sea. Webster et al. [11] have measured a change of 0.535 $\pm$ 0.087 °K/meter per second and 1.257 $\pm$ 0.293 °K/meter per second for vertical and horizontal polarization respectively at 37 GHz and 38° zenith angles. Although these changes were observed from an aircraft below much of the atmosphere and at a smaller zenith angle than the 50° of the Nimbus 6 ESMR, they are indicative of the magnitude of the change in brightness temperature with wind expected in the Nimbus 6 ESMR. Considering the complexity of the emissivity versus wind relationship, there is no gain in accuracy in deviating from the assumption of a linear increase in brightness temperature (as measured in the absence of an atmosphere), and therefore a linear increase in emissivity with wind, at least for winds up to 25 m/sec. With such an assumption

[10] Sabatini, R.R., 1975, Op. Cit.

[11] Webster, W.J. Jr., Wilheit, T.T., Ross, D.B., and Per Gloersen, "Analysis of the Convair-990 Passive Microwave Observations of the Sea States During the Berin Sea Experiment," Paper No. 6 in "Results of the U.S. Contribution to the Joint U.S./USSR Bering Sea Experiment," NASA/GSFC document X-910-74-141, Greenbelt, Maryland, May 1974.

the vertical and horizontal emissivities at 37 GHz can be expressed by:

$$E_v = E_{vo} + a_v W \tag{3.8}$$

$$E_h = E_{ho} + a_h W \tag{3.9}$$

W is wind in m/sec; $a_v = \frac{\Delta Ev}{\Delta W}$ and $a_h = \frac{\Delta Eh}{\Delta W}$ are constants to be determined from observations of T_{Bv} and T_{Bh} in clear areas of known wind, sea-surface temperature, and atmospheric water vapor. This is achieved by plotting observed wind versus E_v (and E_h) as calculated from equations 3.1 and 3.2. Unfortunately, incorrect calibration of Nimbus 6 ESMR data hindered our derivation of reliable a_v and a_h. We can nevertheless estimate a_v and a_h from the airborne microwave observations of Webster et al. [12] at 37 GHz. If we assume that $T_B = ET_s$, their values of 0.535 and 1.257 °K/meter per second for $\Delta T_B/\Delta W$ roughly correspond to vertical and horizontal polarization emissivity changes with wind (a_v and a_h) of 0.002 and 0.004 per meter per second.

Equations for the sea-surface wind can now be obtained by combining 3.2 and 3.8, and 3.1 and 3.4:

$$T_{Bh} = k_o + k_1 E_{ho} T_s + k_1 a_h T_s W_h + k_2 V + k_3 C \tag{3.10}$$

$$T_{Bv} = k_4 + k_5 E_{vo} T_s + k_5 a_v T_s W_v + k_6 V + k_7 C \tag{3.11}$$

In analyzing equations 3.10 and 3.11 we found that the best procedure is to obtain two independent estimates of the wind (W_h and W_v) from estimates of T_s, V, and C. These are then combined into one best estimate $\bar{W}$ by taking the weighted mean of W_h and W_v:

$$\bar{W} = [W_h/\Delta W_h^2 + W_v/\Delta W_v^2]/[1/\Delta W_h^2 + 1/\Delta W_v^2] \tag{3.12 a}$$

The total error $\Delta\bar{W}$ is then obtained from:

$$(\Delta\bar{W})^2 = [(1/\Delta W_h)^2 + (1/\Delta W_v)^2]^{-1} \tag{3.12b}$$

where ΔW_h and ΔW_v are the errors in W_h and W_v.

Let us now briefly examine the accuracy of the above equations for wind determination under specific conditions. We shall assume that $a_v = 0.002$ and $a_h = 0.004$, a U.S. standard atmosphere with V = 2 cm of precipitable water, clear conditions or cloudy conditions with C = 0.04 cm of precipitable water, and $T_s = 290°K$.

For clear atmospheric conditions 3.12 and 3.13 reduce to:

$$T_{Bh} = 118.642 + .857\ W_h + 9.295V \tag{3.13}$$

$$T_{Bv} = 191.760 + .430\ W_v + 4.708V \tag{3.14}$$

[12] Webster et al., 1974, Op. Cit.

when we substitute the constants in Table 3.1, and values of E_{ho} and E_{vo} calculated from equations 3.3 and 3.4. With errors of 1.8°K in T_{Bh} and T_{Bv} and 0.1 cm precipitable water in V, we obtain errors of ± 2.3 m/sec in W_h and ± 4.3 m/sec in W_v, yielding an error of ± 2.0 m/sec (4 knots) in the average wind. If we include a plausible ± 2°K error in the sea-surface temperature, we obtain an error of ± 2.9 m/sec in W_h and ± 4.4 m/sec in W_v, yielding an error of ± 2.4 m/sec (4.8 knots) in the average wind.

When we consider the above situation with cloudy conditions, equations 3.10 and 3.11 reduce to:

$$T_{Bh} = 130.155 + .662\ W_h + 7.046\ V + 624.65\ C \qquad (3.15)$$

$$T_{Bv} = 196.122 + .334\ W_v + 4.015\ V + 351.63\ C \qquad (3.16)$$

With errors of 2.7°K in T_{Bh}, 1.7°K in T_{Bv}, 0.1 cm precipitable water in V, 0.01 cm precipitable water in C, and 2°K in sea-surface temperature, we obtain errors of ± 10.3 and ± 11.9 m/sec in W_h and W_v, which then combine to yield a total error of 7.8 m/sec (16 knots) in the average wind. The error in cloud precipitable water C is the biggest contributor to the total error; even if we halve this error to 0.005 cm precipitable water we would still obtain a total error of 4.9 m/sec (10 knots). Figure 3.4 summarizes the errors in the wind estimates obtained from equations 3.10 and 3.11 for clear and cloudy atmospheres approximating the U.S. standard atmosphere.

The preceding error analysis assumes no errors in T_B measurements, does not include errors in the emissivity versus wind linear relationship as expressed by equations 3.8 and 3.9, nor any inaccuracies introduced by the thin-atmosphere assumption and errors in atmospheric absorption coefficients in the derivation of 3.10 and 3.11. All of these factors would tend to increase the wind estimate errors. Instrument errors in T_B measurements can be attenuated by averaging two or more values of T_B's; errors in the emissivity versus wind relationship could be minimized by including other parameters such as fetch and air stability; finally the errors of the thin-atmosphere assumption and errors in the use of equations 3.1 and 3.2 for T_B can be eliminated (especially in the case of a cloudy atmosphere) by solving the radiative transfer equation for surface emissivity. In the solution of the radiative transfer equation we seek a surface emissivity E_s which "fits" estimated or measured values of atmospheric parameters and satellite-measured T_B. The determination of this surface emissivity is therefore an iterative computational process which starts with a best estimate of E_s. Unless we have very accurate measurements of atmospheric parameters, such an approach would yield no better results than the regression equation approach we have used to solve for surface emissivity (i.e., equation 3.1 and 3.2). With our proposed approach, in a clear atmosphere where the thin atmosphere approximation is most accurate the wind estimate errors in open seas (fetch unlimited situation) may be kept to acceptable levels (± 5 knots) by good estimates of atmospheric water vapor (to within 5-10% of total), sea-surface temperatures to within 2°K, and by averaging two or more values of T_B's to attenuated instrument

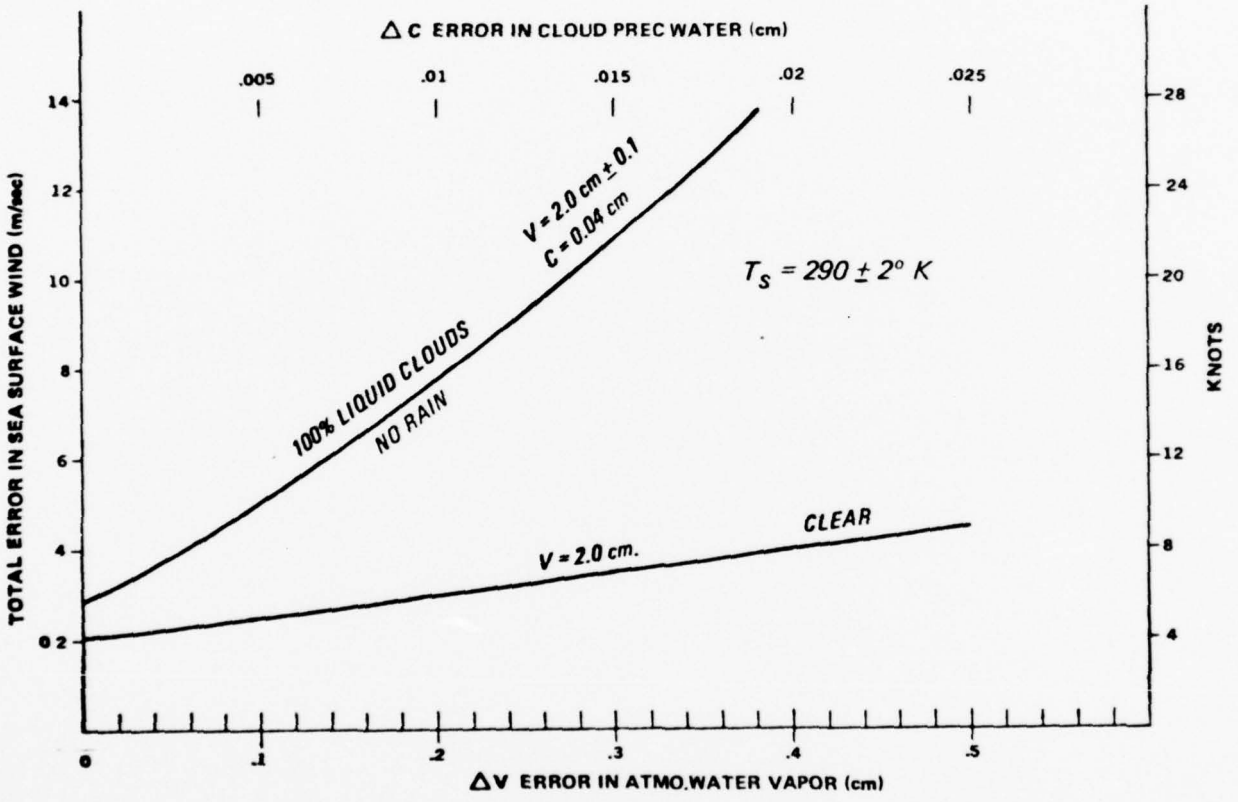

Figure 3-4 Errors in sea-surface wind estimates using equations 3.12 and 3.13 for a clear and cloudy atmosphere approximating a U.S. Standard Atmosphere. The lower horizontal scale represents the error in water vapor content, ΔV, for a clear atmosphere. The upper horizontal scale represents the error in cloud precipitable water, ΔC, for a 100% cloudy atmosphere. An error of ± 0.1 cm of water vapor content V is assumed for the cloudy atmosphere, and of ± 2°K in sea-surface temperature for both atmospheres.

errors. Such estimated wind accuracies with the Nimbus 6 ESMR are based only on the analyses we just presented; verification must await availability of correctly calibrated Nimbus 6 ESMR data.

In the case of a cloudy (liquid) non-precipitating atmosphere wind estimate errors of ten knots or greater may be unacceptable. In this situation an iterative solution of the transfer equation to obtain E_s may be warranted, but only if accurate estimates of cloud water content are available.

In rain situations good sea-surface wind estimates are probably unattainable because rain mostly obliterates microwave radiation from the surface to space, and therefore masks the effects of surface emissivity changes caused by wind. Figure 3.5 shows the rainfall absorption coefficients at 19.35 GHz (1.55 cm) and 37 GHz (0.81 cm) as calculated from equations given by Paris [13]. At 37 GHz rain absorbs more than twice than at 19.35 GHz, and even light rain would quickly mask the surface to the 37 GHz radiometer.

The accuracy of sea-surface wind determination in clear and cloudy areas may be improved if additional microwave channel measurements are available. Wilheit et al. [14] have used observed brightness temperatures from an airplane flying above the Bering Sea measured in five microwave channels (from 0.81 to 2.8 cm) to derive estimates of the wind to within 1.4 m/sec even in cloudy areas. The technique they employed involves the solution (in a least square sense) of five equations similar to 3.10 and 3.11. Such an approach from orbital heights will be possible with a satellite carrying multichannel microwave sensors. Presently, to test this approach one could take advantage of the Nimbus 5 ESMR at 19.35 GHz, which when operative has nearly simultaneous coverage of the same areas scanned by the Nimbus 6 ESMR. The 19.35 GHz T_B would provide an additional equation of the form of 3.10 and 3.11. Assuming that such an equation yields a wind estimate with a standard error of about eight knots (four m/sec), when this wind estimate is combined to the 37 GHz channel wind estimates with standard errors of 2.9 and 4.4 m/sec, we obtain a wind estimate with a standard error of about two m/sec (four knots). In cloudy non-precipitating areas an additional Nimbus 5 ESMR wind equation having errors comparable to the two Nimbus 6 ESMR equations (10.3 and 11.9 m/sec) would reduce the total wind error to about six m/sec (12 knots). The verification of the accuracy of such a three-channel approach must also await the availability of correctly calibrated Nimbus 6 ESMR data.

[13] Paris, J.F., 1971, Op. Cit.

[14] Wilheit, T.T., Fowler, M.G., Stombach, G., and Per Gloersen, "Microwave Radiometric Determination of Atmospheric Parameters During the Bering Sea Experiment," Paper No. 5 in "Results of the U.S. Contribution to the Joint U.S./USSR Bering Sea Experiment," NASA/GSFC document X-910-74-141, Greenbelt, Maryland, May 1974.

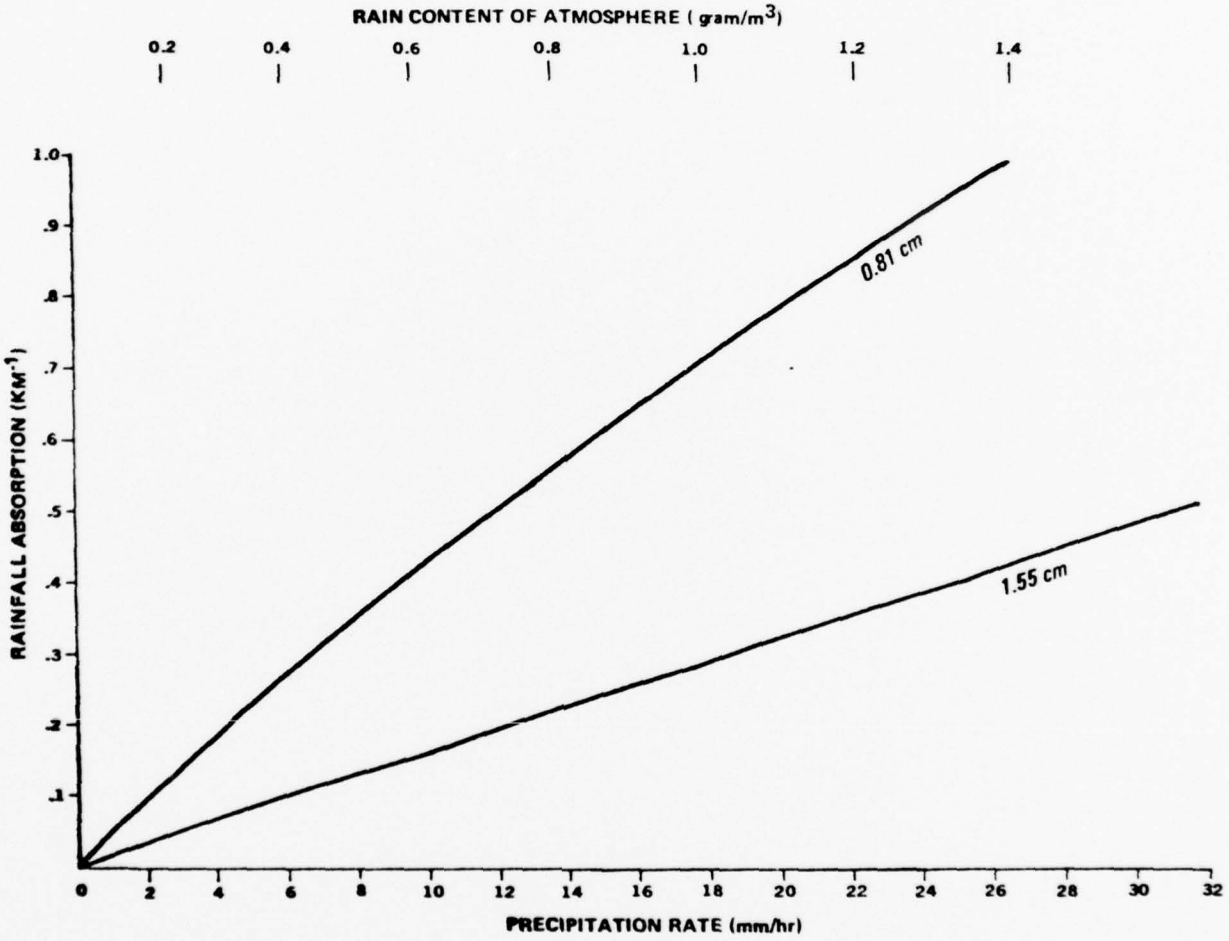

Figure 3-5 Rainfall absorption coefficients as a function of precipitation rates and rain content of atmosphere for 0.81 cm (37 GHz) and 1.55 cm (19.35 GHz) radiation. Calculations were performed with equations given by Paris (1971). Rain content and precipitation rates are related by the Marshall-Palmer raindrop distribution (1948).

4.0 NIMBUS 6 ESMR OBSERVATIONS OF BRIGHTNESS TEMPERATURES

A search for usable ESMR data over the oceans was conducted using the files of ESMR images available at NASA/GSFC, Greenbelt, Maryland, and surface weather maps. We concentrated this first search to the North Atlantic, an area of dense wind observations and frequent cyclonic storms, even in the summertime. The ESMR data selected from this first search covering only the 1975 summer months were finally received from NASA at the end of December 1975, six months after Nimbus 6 launch. Since these summer month data contained few observations of high winds above 40 knots, we conducted a second search and put in another order at NASA for selected ESMR data over the North Atlantic during the fall and winter of 1975-1976. Additionally, we ordered ESMR data covering a few possible Mistral occurrences in the Mediterranean sea.

All data were received in the Calibrated Brightness Temperature Tape (CBTT) format and were mapped out with our mapping program. Maps of T_{Bv}, T_{Bh}, and $T_{Bv} - T_{Bh}$ were produced. Latitude-longitudes were drawn on the maps with the aid of rubber grids. Three Nimbus 6 daytime passes over the North Atlantic were selected on the basis of high winds and good wind reports from the first group of ESMR data.

Analyses of wind and brightness temperatures in clear and cloudy areas were conducted from the mapped T_B data and wind observations on the closest six-hour surface maps.

As we proceeded in the analyses we noticed that observed brightness temperatures did not quite correspond to those obtained by calculations with the atmospheric models described in the Appendix. The differences were especially evident in clear land and oceanic areas in which the observed T_{Bv} and T_{Bh} seemed to be 10-20°K lower than the calculations. As illustrative examples of typical T_B values obtained from the Nimbus 6 ESMR, we shall present a few scans covering clear and cloudy areas as shown by the SMS and NOAA satellite imagery. Figure 4-1 is a sector of an SMS image of the U.S. East Coast and Atlantic areas on which is outlined the Nimbus 6 ESMR coverage, and two paths of averaged ESMR scans. Each swath represents the coverage of three scans, the averages of which are shown in Figures 4-2a and 4-2b. The northern-most three-scan swath (Figure 4-2a) starts over land, crosses the Delmarva Peninsula, skirts the New Jersey coast, and covers clear and cloudy areas over the Atlantic. T_{Bh} and T_{Bv} reach 258°K and 270°K respectively over land, average 124°K and 192°K in clear ocean areas south of Long Island, and reach up to 240°K and 260°K over rain clouds.

The southernmost swath (Figure 4-2b), except for some clouds in the middle part, is mostly over clear oceanic areas. T_{Bh} and T_{Bv} over clear areas range from 122-130°K and 196-200°K respectively left of center, and from 125-145°K and 196-206°K right of center. Ocean brightness temperatures are higher than those recorded south of Long Island, most likely because of higher ocean temperatures and high atmospheric water content south of the cold front. A gradual decrease of brightness temperature away from the center of the swath is apparent, especially in the T_{Bh}.

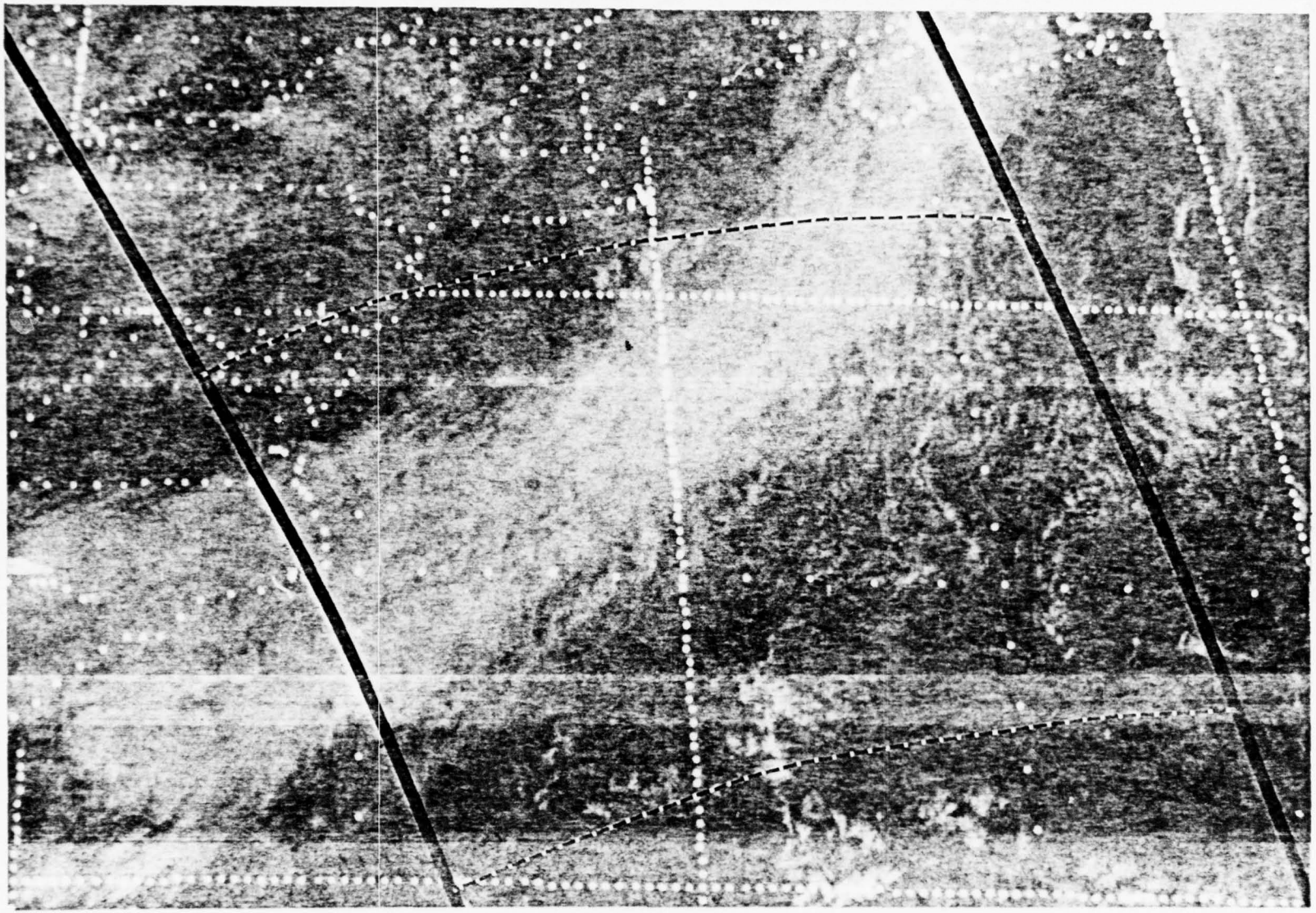

Figure 4-1 Synchronous Meteorological Satellite (SMS-1) image of the U.S. East Coast area taken on 13 September 1975, 1400 GMT. On the image is outlined the Nimbus 6 ESMR coverage occurring at about 1550 GMT of the same day. The two dashed lines represent the position of ESMR scan lines averaged in Figures 4-2a, b.

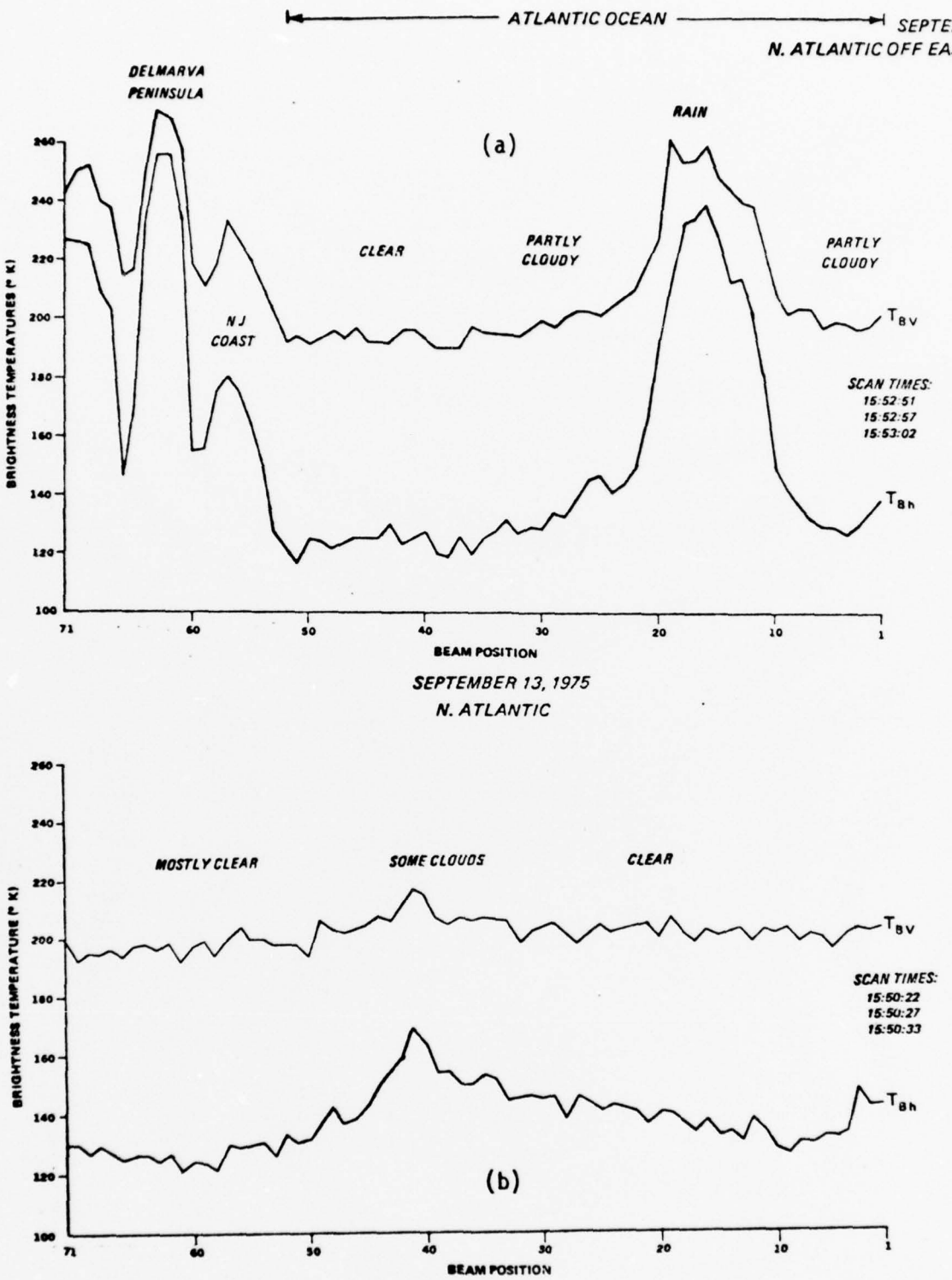

Figure 4-2 Average horizontal and vertical brightness temperatures of three scan lines occurring over the U.S. East Coast and Atlantic area at about 40°N (a), and at about 32°N (b). The position of the two sets of scan lines is also shown on the SMS-1 image in Figure 4-1.

For comparison to the observed T_B's we call attention to Figure 3-1 which shows the results of T_B calculations for a U.S. standard atmosphere and sea-surface temperature of 290°K obtained by our thin atmosphere approximation (see Appendix). These calculations yield clear areas T_{Bv} and T_{Bh} values of about 204°K and 144°K at vertical and horizontal polarization sea-surface emissivities of 0.61 and 0.34. These are 12° and 20°K higher than the comparable Nimbus 6 ESMR averages of 192°K and 124°K south of Long Island. Other data checks with calculations made with our atmospheric model, comparisons of our model results to calculations performed by Stogryn [15], and to calculations made with formulas given by Paris [16] at 55° Nadir, also indicated that the Nimbus 6 ESMR produces T_{Bv} and T_{Bh} 10-20°K lower than what they should be. Subsequent conversations with NASA officials at GSFC, who at about the same time (May 1976) were experiencing the same difficulty with the data, confirmed our suspicions. According to Dr. Wilheit [17] the ESMR experimenter, the problem is due to the heating of the sun shining on the microwave antenna causing an erroneous calibration of the instrument. NASA is presently working on deriving a corrected calibration which would eliminate this heating effect. An analysis we conducted with some of the data shows that this calibration error is more pronounced in the horizontal polarization, and is a function of beam position (which determines antenna aspect position relative to sun). Figure 4-3 presents T_{Bv} and T_{Bh} values averaged for each beam position for swaths spanning the south and north Atlantic Ocean. To eliminate thick clouds and rain areas which would introduce gross deviations in these limited area averages, we included only T_{Bh} below 170°K and T_{Bv} below 210°K. The four swaths, two in the daytime (24 November 1975, 29 February 1976) and two in the nighttime (14 December 1975, 21 February 1976) were chosen at random from the ESMR data we had ordered from NASA. All averages show a peak near the center of the swath, a steep decrease away from the center, and a small rise near the edges. For this limited data sample, the peak-to-trough variations are about 7-11°K for T_{Bv} and 12-17°K for T_{Bh}, with the data near the center of the scan containing the least relative errors. The corrections to be applied are obviously a function of antenna position relative to the sun, which in turn is determined by beam position, latitude, and time of year. No attempt was made in our work to correct for this calibration error.

Calibration errors render impossible the use of the Nimbus 6 ESMR data for deriving valid relationships between sea-surface winds and brightness temperatures. Nevertheless, as a preliminary effort to evaluate the data at hand for sea-surface wind estimation we have considered the analysis of a Mistral occurrence in the Mediterranean sea

[15] Stogryn, A., 1972 Op. Cit.

[16] Paris, J.F., 1971, Op. Cit.

[17] Communication with Dr. T. Wilheit, May, 1976.

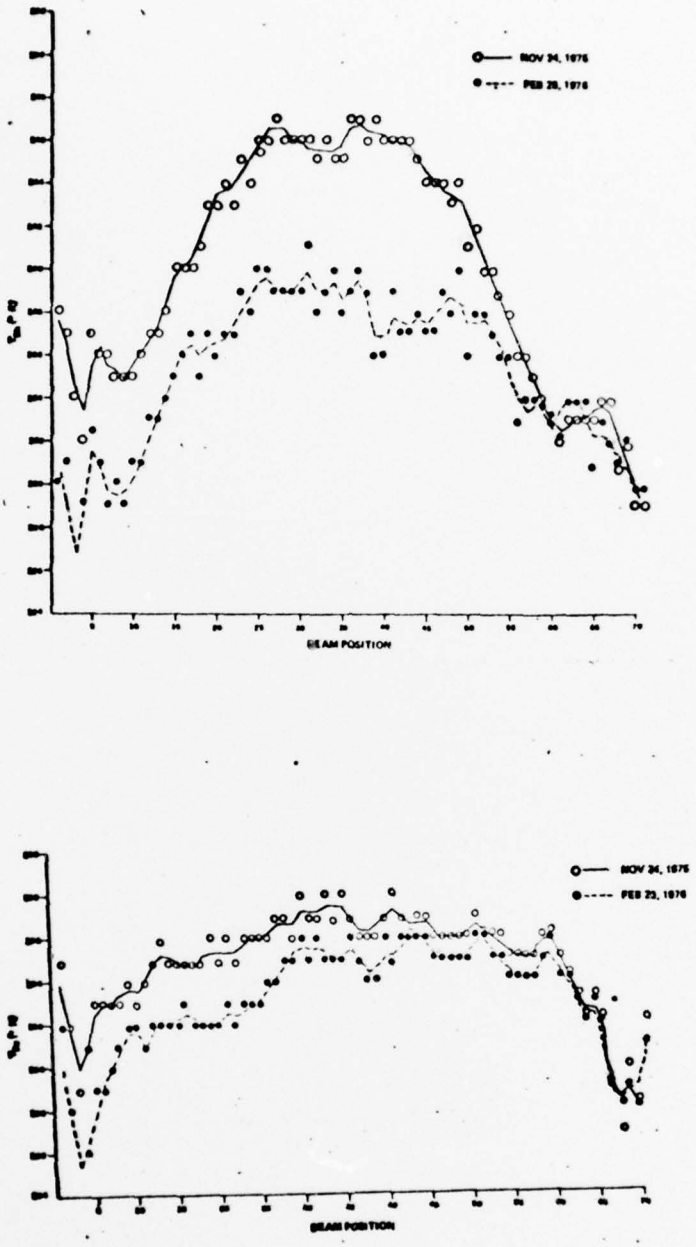

Figure 4-3 Average brightness temperatures as a function of beam position for four Nimbus 6 ESMR swaths spanning the south and north Atlantic ocean. The four swaths, two in the daytime (24 November 1975, 29 February 1976) and two in the nighttime (14 December 1975, 21 February 1976) were chosen at random from ESMR data furnished by NASA. The solid and dashed lines represent 1-2-1 smoothing of the actual averages.

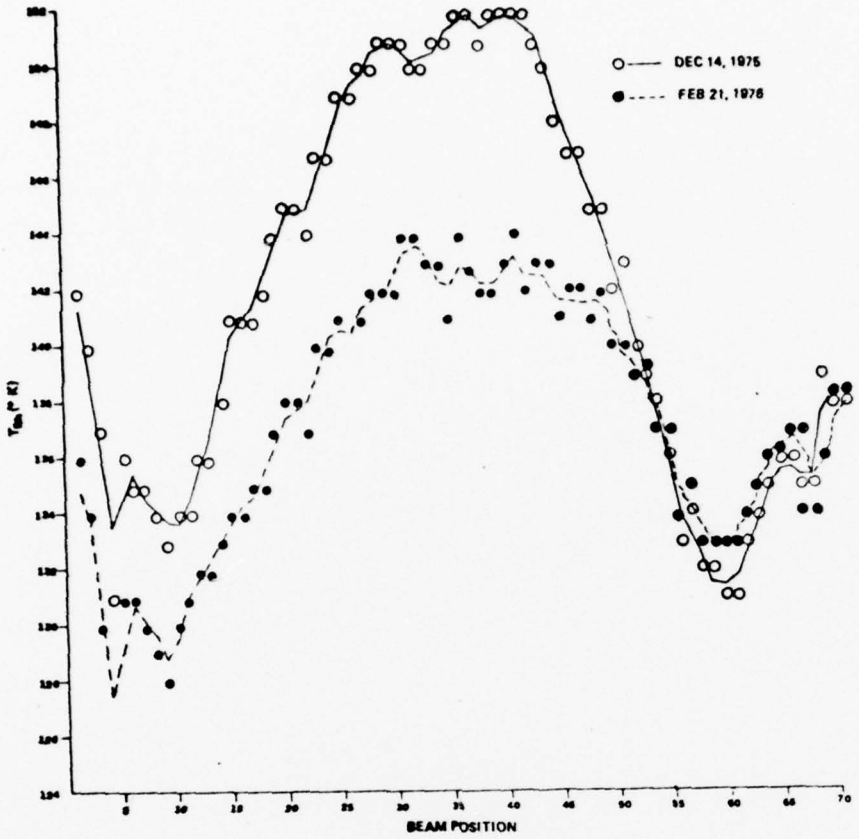

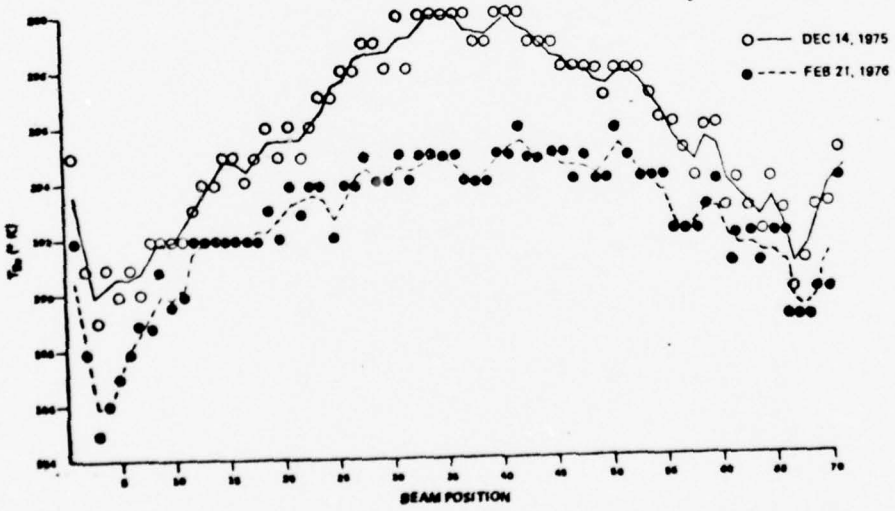

Figure 4-3 Continued

and the analysis of large area averages of wind versus T_B. The large area analysis would attenuate the calibration errors.

We shall first present a Nimbus 6 ESMR coverage of a Mistral occurrence on 15 January, 1976, because it is probably the most convincing evidence we have that Nimbus 6 ESMR can be used for sea-surface wind determination. Figure 4-4 and 4-5 show the gridded T_{Bh} and T_{Bv} maps obtained from a Nimbus 6 pass over the Mediterranean on 15 January 1976, between 10:31 and 10:33 GMT. Recorded on the maps are the reported winds at 1200 GMT which range up to 45 knots. Figure 4-6 is a NOAA satellite image of the area taken at 8:48 GMT, on which is outlined the ESMR coverage. The surface weather map for 12 GMT, 15 January (Figure 4-7) contains the typical Mistral synoptic conditions with a large anticyclone centered over western Europe and the Atlantic and a trough crossing the Italian peninsula. Both the T_{Bh} and the T_{Bv} maps show an area of relatively higher temperatures in the Gulf of Lion, yet the NOAA satellite image and the 1200 GMT surface map show little or no clouds in the area. Available ship reports at 1200 GMT show one- to two-tenths cirrus and one-tenth cumulus, which would hardly affect the brightness temperatures.

Relatively higher brightness temperatures in the Gulf of Lion area during Mistral occurrences have also been reported in a previous study with Nimbus 5 ESMR [18], and are thought to be caused by the higher winds of the Mistral funneling into the Gulf of Lion and causing rougher seas in this area. Ships in and around the area of the Mistral reported winds of 35 to 45 knots. In one instance, near the coast of France at about 41.5N and 3.4E, the high wind report is not reflected by higher T_B's. One may think that calibration errors and the 88 minutes difference between the wind observation and the T_B map could be the cause of such discrepancy. A more likely explanation is the nearness of land, a reminder that what the ESMR "sees" is only the effect of the wind upon the waters, i.e. waves, foam, and spray. Near the coastline where the fetch is short, the effect of the Mistral wind upon the waters is not as pronounced as in the open seas and therefore T_B's are not as high.

Figure 4-8 represents the average T_{Bh} and T_{Bv} of three scans across the Mistral area (see Figure 4-7). These averages also bring out the effect of the Mistral in the Gulf of Lion, which is evidenced by nearly 25°K and 20°K increases in the T_{Bh} and T_{Bv} averages respectively. Partially masking and distorting the Mistral effect is of course the calibration error. If we can assume that the curves shown in Figure 4-3 are representative of the relative calibration error across beam positions 1 to 71, then the calibration error would emphasize the Mistral effect near the left edge (beams 65-53) by steepening the west-east T_B gradient here by about 4-6°K; and would de-emphasize the effect west of the apparent T_B maximum (beam 53) by lessening the east-west T_B gradient by about 4-5°K in the following 12 beam positions (52-41).

[18] Sabatini, R.R., 1974, Op. Cit.

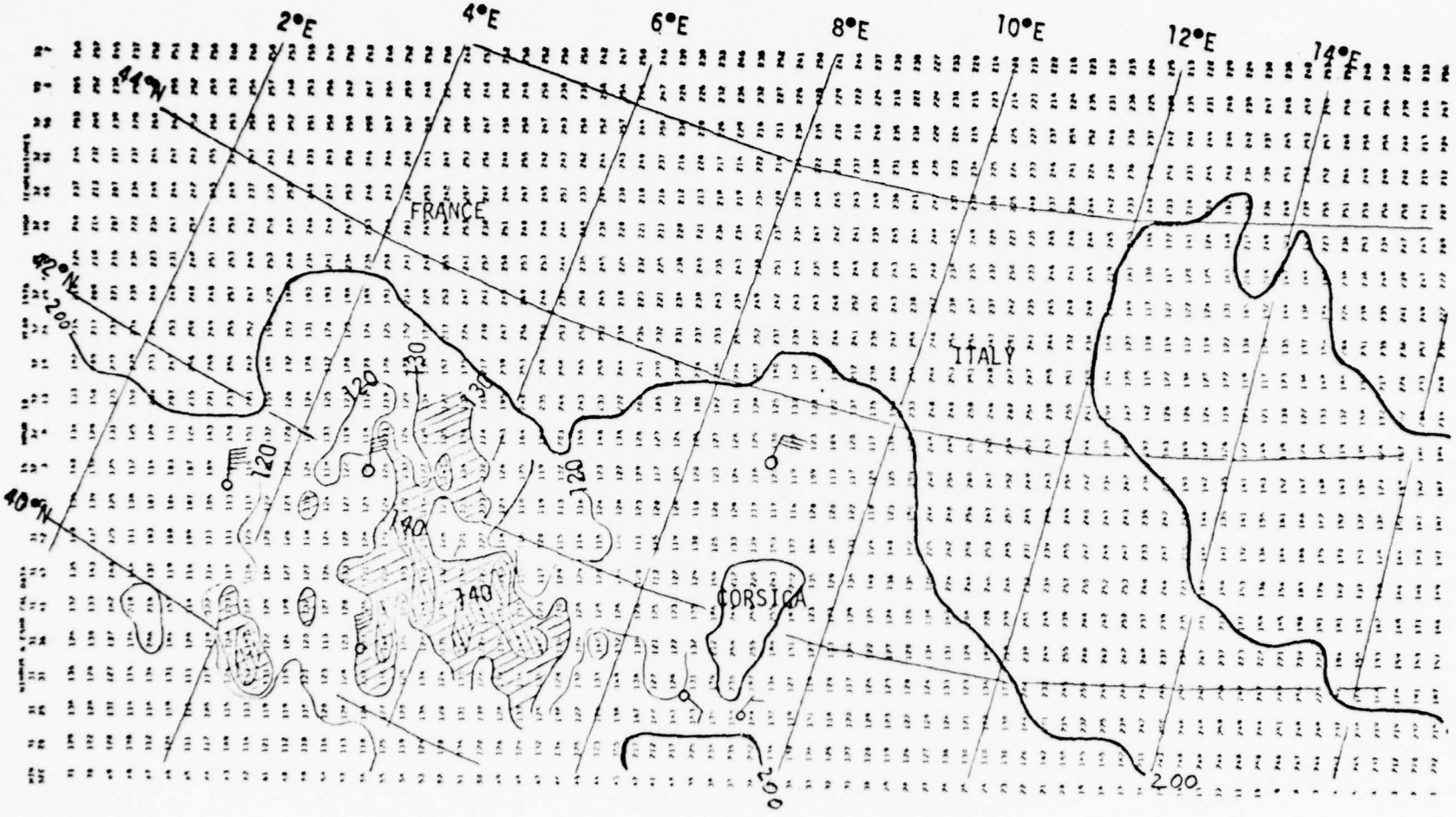

Figure 4-4 Nimbus 6 ESMR horizontal brightness temperature maps of the Mistral area taken on 15 January 1976 between 10:31:20 GMT and 10:33:07 GMT. ESMR area coverage is also shown on the NOAA satellite image in Figure 4-6.

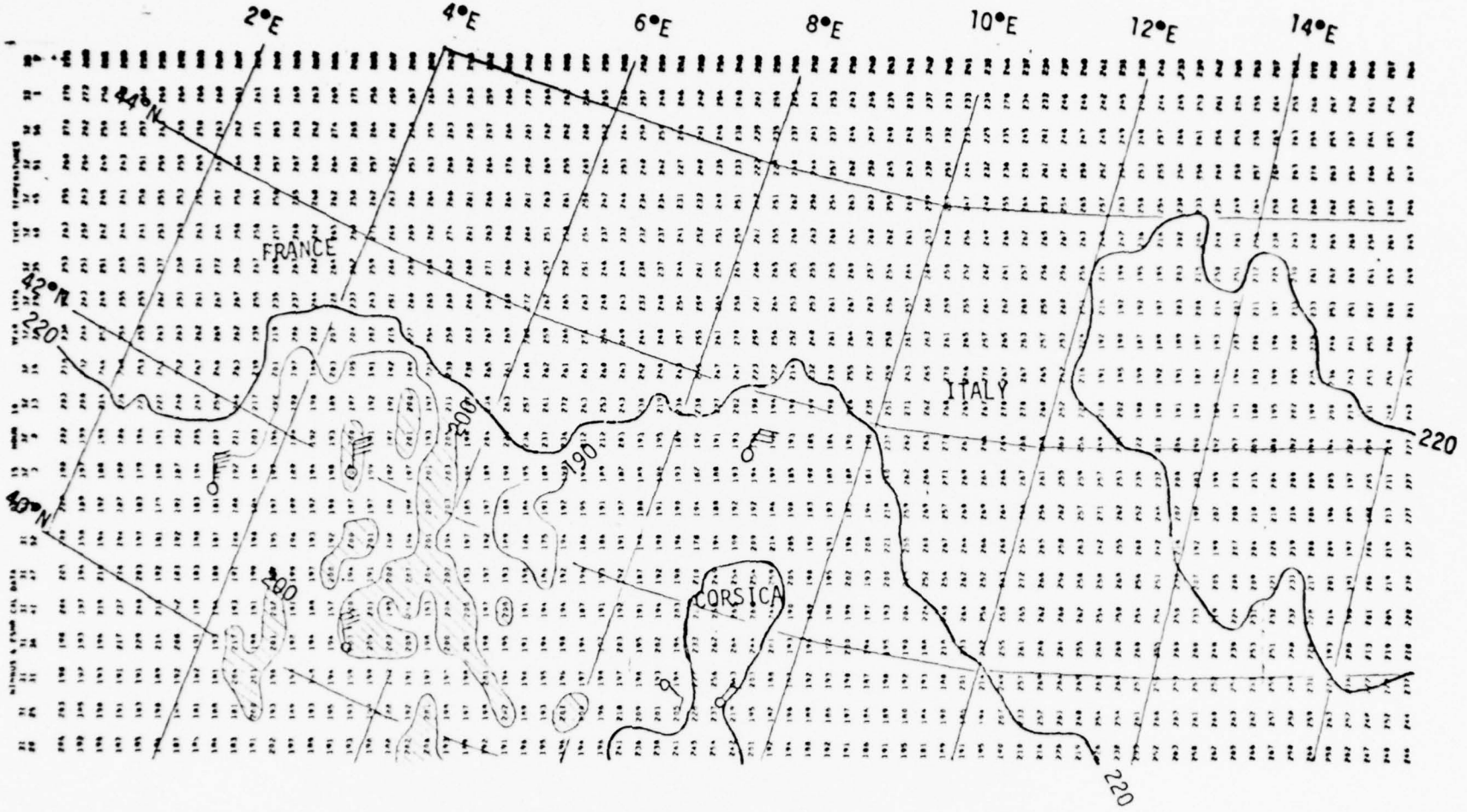

Figure 4-5 Nimbus 6 ESMR vertical brightness temperature map of the Mistral area taken on 15 January 1976 between 10:31:20 GMT and 10:33:07 GMT. ESMR area coverage is also shown on the NOAA satellite image in Figure 4-6.

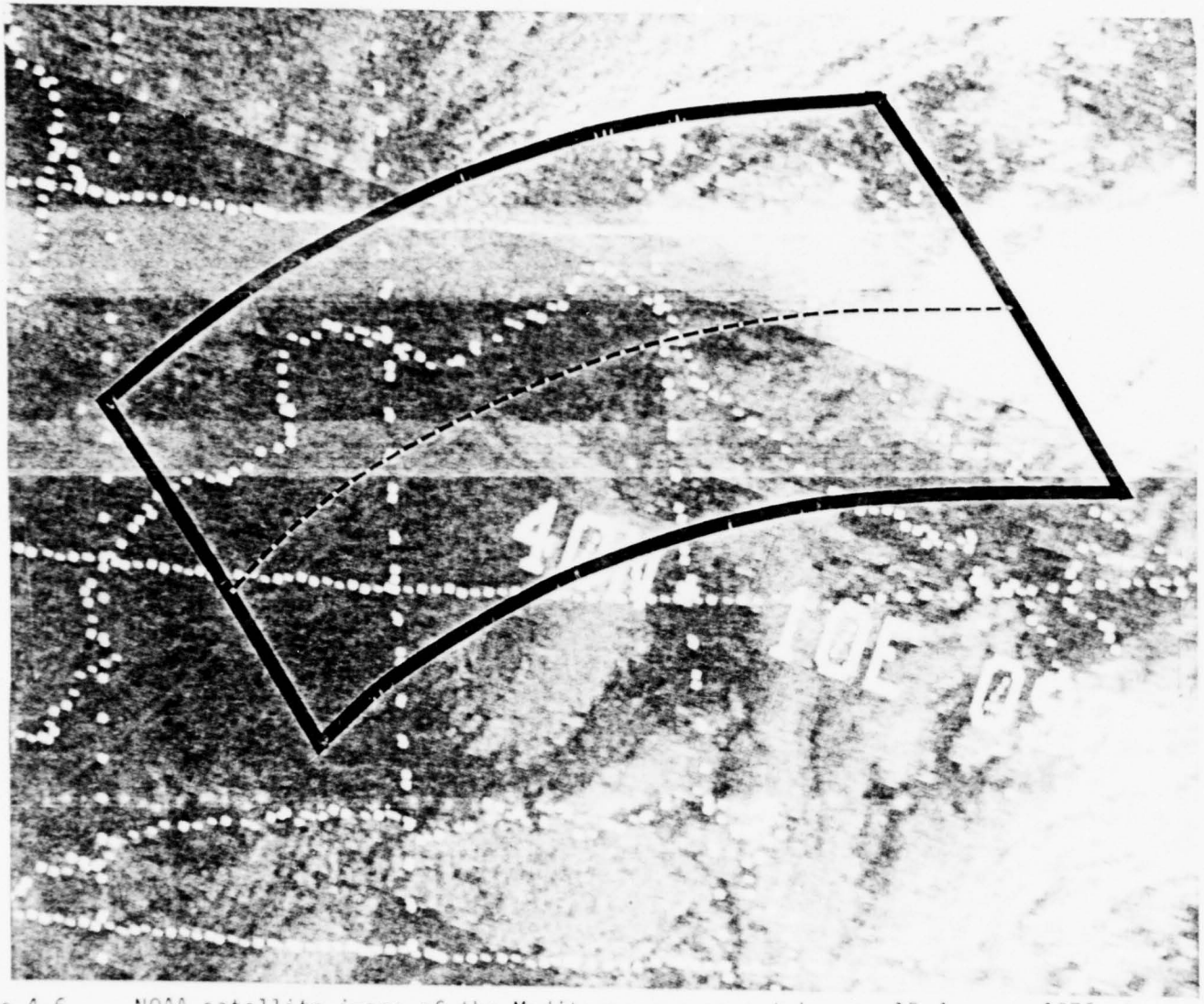

Figure 4-6 NOAA satellite image of the Mediterranean area taken on 15 January 1976 at 0848 GMT. On the image is outlined the Nimbus 6 ESMR coverage mapped in Figures 4-4 and 4-5. The dashed line represents the position of three ESMR scan lines whose averages are shown in Figure 4-8.

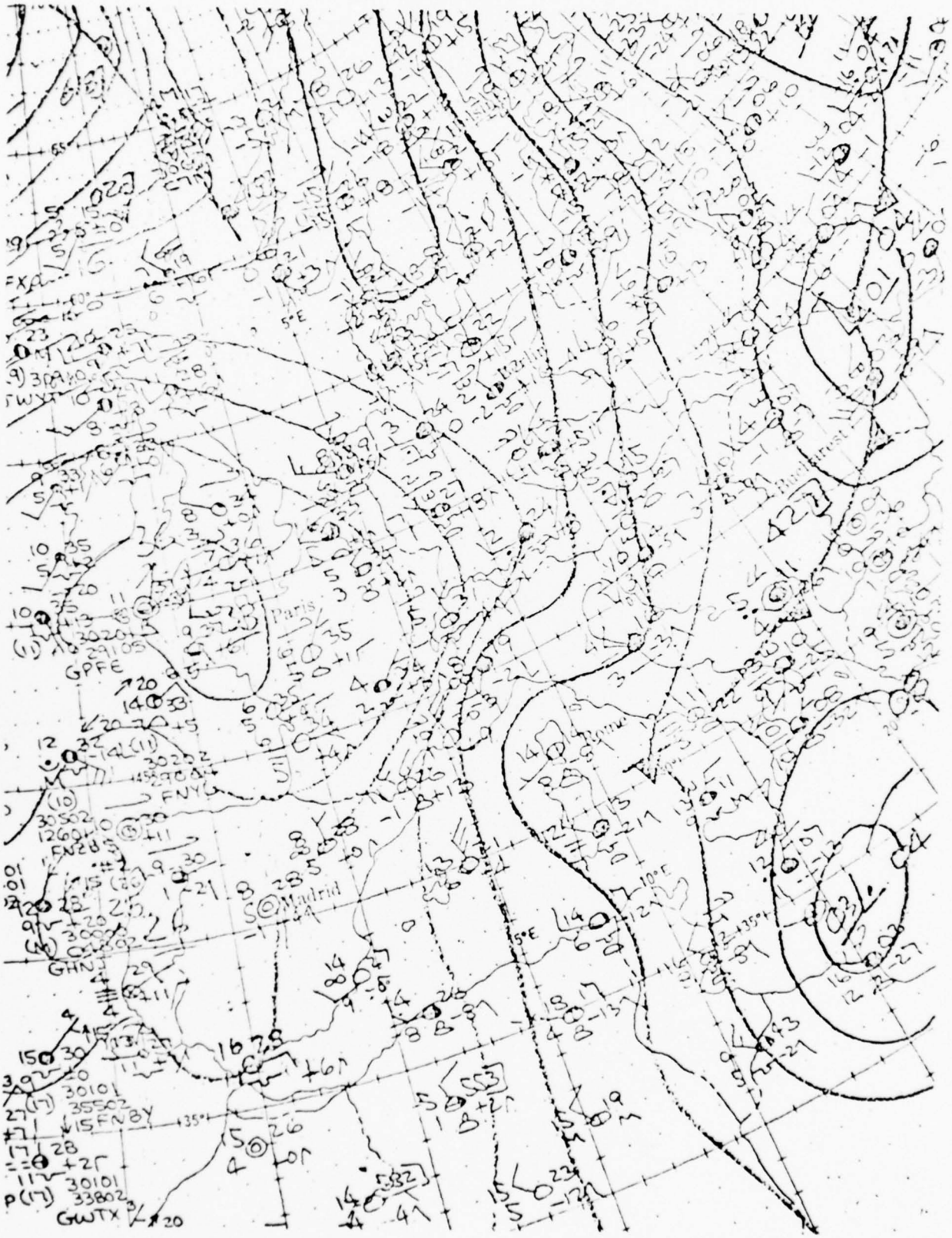

Figure 4-7 Surface weather map for 1200 GMT 15 January 1976.

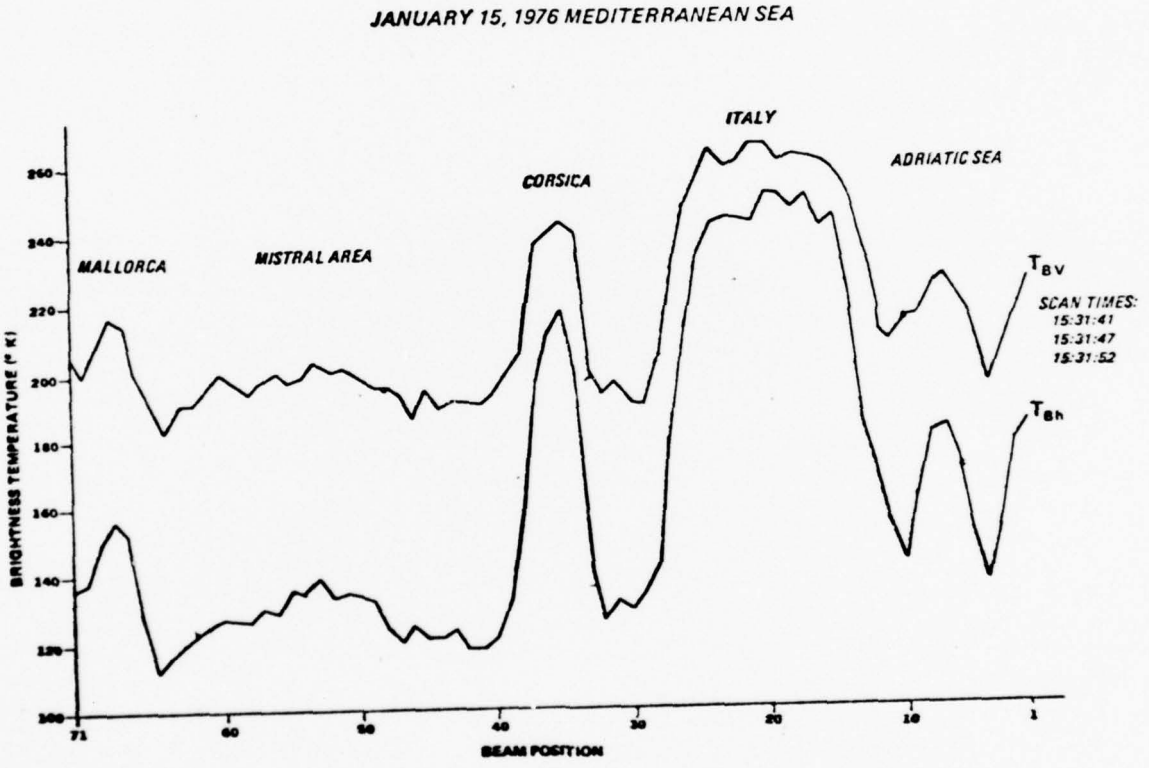

Figure 4-8 Average horizontal and vertical brightness temperatures of three scan lines crossing the Mistral area on 15 January 1976. The position of the scan lines is also shown on the NOAA satellite image in Figure 4-6.

Because of calibration errors and insufficient wind data, no quantitative evaluation of T_B versus wind is possible from this single Mistral event. Nevertheless, this Mistral occurrence does show a pronounced effect on 37 GHz brightness temperatures similar to the effect observed on the 19.35 GHz T_B's in other Mistral occurrences, and indicates that further analyses with correctly calibrated 37 GHz T_B data may yield useful statistical relationships between wind and T_B's.

The next analysis involves large area comparisons of wind and brightness temperatures.

Three Nimbus 6 ESMR daytime passes over the North Atlantic were selected for this analysis from the first batch of ESMR data received from NASA at the end of December 1975. The selection was made on the basis of high winds and good wind reports. The passes occurred on 5 August, 11 September, and 13 September 1975. Maps of T_{Bv}, T_{Bh}, and $T_{Bv} - T_{Bh}$ covering the North Atlantic area were produced with our mapping program and gridded. The ESMR data which were mapped occurred from about 12:20 to 12:30 GMT on 5 August, from about 13:45 to 13:55 GMT on 11 September, and from about 15:45 to 15:55 GMT on 13 September. Surface winds over the ocean were estimated from observations and from pressure gradients by means of the geostrophic approximation corrected for surface friction. The 12:00 GMT surface maps and wind observations were used for the August 5 and September 11 cases. Both the 12:00 GMT and the 18:00 GMT maps were used to interpolate the position of the isobars for the time of the September 13 ESMR data (about 16:00 GMT).

Isotachs were drawn at five- and ten-knot intervals and transferred to the gridded T_B maps. Average $T_{Bv} - T_{Bh}$ were then calculated for the area enclosed by each ten-knot interval (or five-knot interval where wind data warranted it). Figure 4-9 shows a plot of the results. Each point is an average $T_{Bv} - T_{Bh}$ plotted against the middle of the wind interval; i.e., the average of all $T_{Bv} - T_{Bh}$ falling within 0-to 10-knot isotachs were plotted at 5 knots, etc. The graph in Figure 4-9 shows the expected decrease in $T_{Bv} - T_{Bh}$ as the wind increases. However, great caution should be used in interpreting these results. First of all, no allowances were made for the calibration error discovered after this analysis was completed; second and most importantly, the averages include data over all clear, cloudy, and rain conditions. The correspondence between $T_{Bv} - T_{Bh}$ and wind, if any, may therefore be hidden by the fact that there is an increase in cloudiness and precipitation in areas where one also expects an increase in wind (toward the center of a low pressure system). Clouds and rain lessen the contribution of the surface polarized radiation, and therefore tend to attenuate $T_{Bv} - T_{Bh}$.

Figure 4-10 a,b shows the average T_{Bv} and T_{Bh} plotted against the middle of the wind interval for the August 5 case only. Since the calibration error was discovered at about the time of this analysis, we decided not to proceed with further analyses on the other two cases. Again, although both T_{Bv} and T_{Bh} show the correct trend with wind, we cannot come to any firm conclusion because of the inclusion of cloud areas. A valid analysis of T_B versus wind must await correct calibration of the data, and should exclude cloud-covered areas. For such an analysis, clear areas can best be determined by temperatures obtained from the Temperature Humidity Infrared Radiometer (THIR), also flying on the Nimbus 6 satellite.

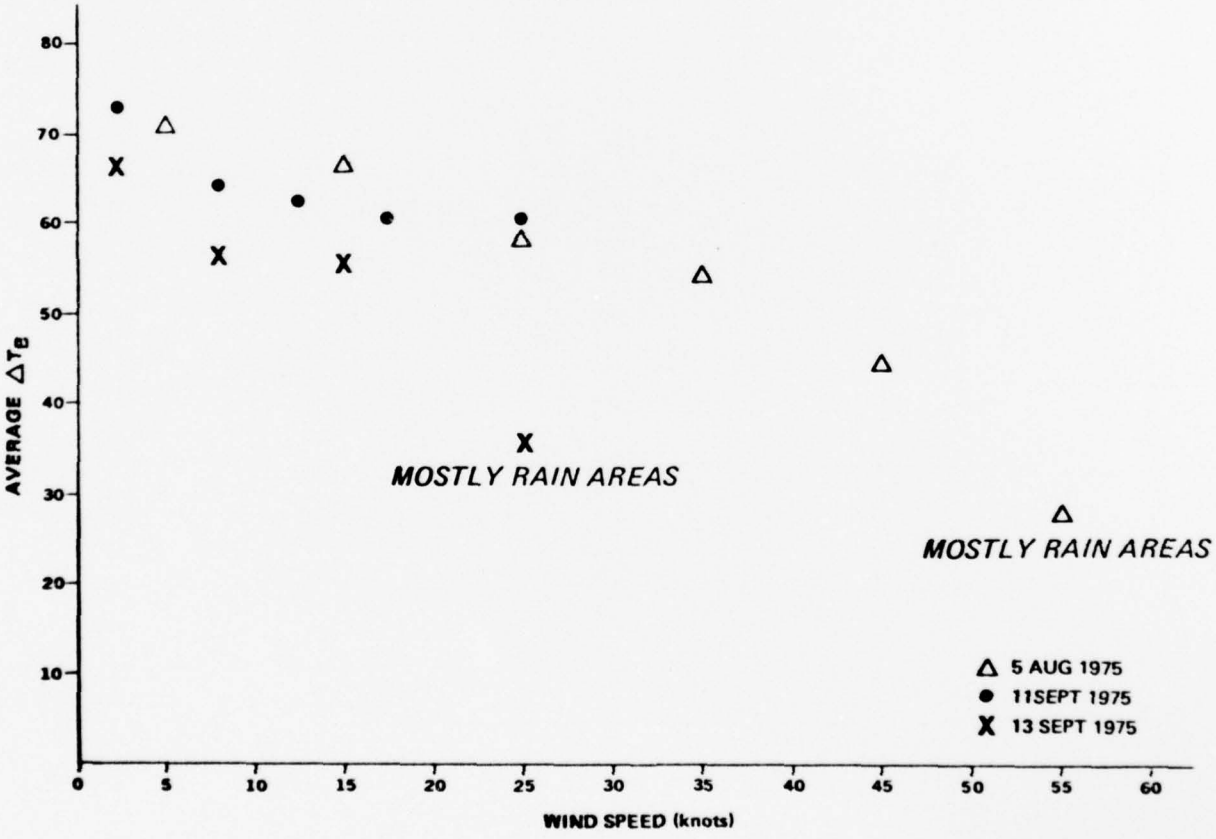

Figure 4-9 Plot of large area averages of $T_{Bv} - T_{Bh}$ as a function of wind. The ESMR data used in this analysis occurred over the North Atlantic from about 12:20 to 12:30 GMT on 5 August 1975, from about 13:45 to 13:55 GMT on 11 September 1975, and from about 15:45 to 15:55 GMT on 13 September 1975.

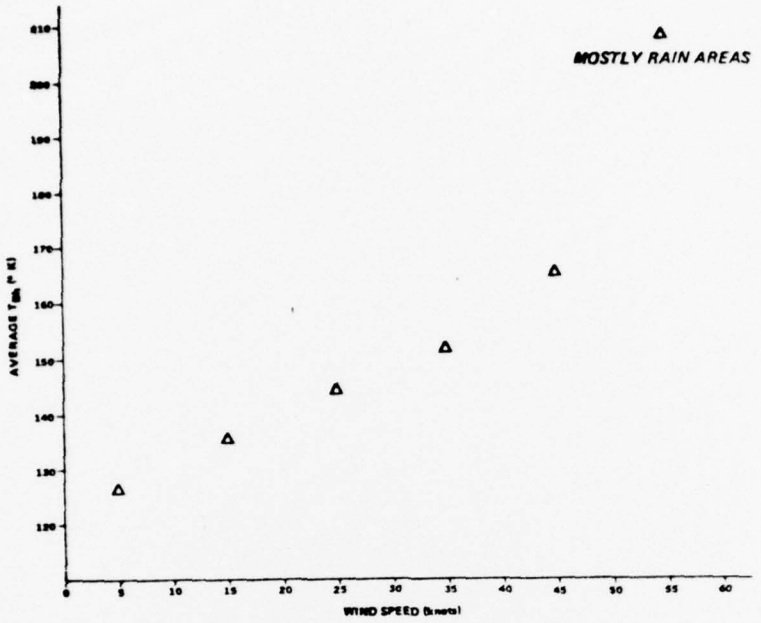

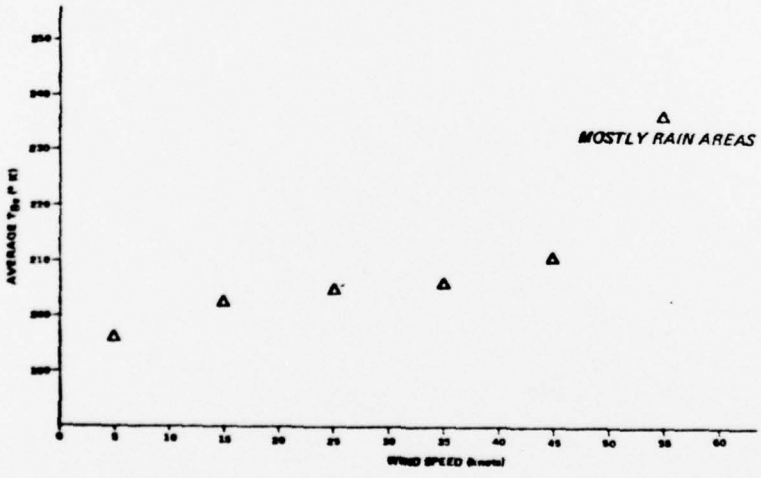

Figure 4-10 Plot of large area averages of T_{Bv} and T_{Bh} as a function of wind for the North Atlantic on 5 August 1975.

5. CONCLUSIONS AND RECOMMENDATIONS

The presence of a calibration error has prevented a quantitative evaluation of the applicability of the Nimbus 6 ESMR to sea-surface wind determination. Comparisons of T_B's produced by the Nimbus 6 ESMR to T_B's calculated over model atmospheres show that calibration errors cause T_{Bv} and T_{Bh} to be 10-20 °K lower than what they should be. The error is determined by the sun-antenna angle, and therefore shows up as a function of antenna beam position with the error increasing toward the horizons.

A preliminary error analysis on wind equations which assume a linear relationship between wind and sea-surface emissivities shows that in open, well-developed seas, surface winds less than 50 knots may be estimated from Nimbus 6 ESMR to an accuracy of about 5 knots in clear areas and 10 to 16 knots in cloudy non-precipitating areas. The addition of Nimbus 5 ESMR data would improve the wind estimates to an accuracy of 4 knots in clear areas and 7 to 11 knots in cloudy non-precipitating areas. These accuracies can further be improved by solving for surface emissivities by iterative solutions of the microwave radiative transfer equation; this method is warranted only if atmospheric parameters are accurately known.

The high sensitivity of the Nimbus 6 ESMR to rain precludes its use for sea-surface wind estimation in rainy areas.

The analysis of Nimbus 6 ESMR T_B's during a Mistral occurrence shows that even in the presence of a calibration error the Nimbus 6 ESMR can qualitatively detect the effect of the wind upon the sea. This effect causes relatively high horizontal and vertical brightness temperatures in areas of expected higher winds. Large area analysis of T_B's and wind also show increases in T_{Bv} and T_{Bh} with wind, and a decrease in $T_{Bv} - T_{Bh}$. This large area analysis is nevertheless inconclusive, because of the natural presence of an increase in cloud cover and rain with winds, which also increase T_B's.

It is concluded that T_B's versus winds analyses should be pursued further when correctly calibrated Nimbus 6 ESMR data are available. Concurrent Nimbus 5 ESMR data should also be used to derive and test an improved set of three wind estimation equations.

Analyses for deriving sea-surface emissivity versus wind equations should concentrate on clear areas in which atmospheric effects can be best corrected for. Advantage should be taken of simultaneous Nimbus THIR measurements for determining clear areas.

The wind equations derived by the proposed method involving best-fit equations of T_B versus surface and atmospheric parameters should be tested against a second method employing iterative solutions of the microwave radiative transfer equation for surface emissivity. Tests should be made over clear and cloudy non-precipitating areas in which surface winds and radiosonde ascents are available.

REFERENCES

NASA, Goddard Space Flight Center, Greenbelt, Maryland, 1975. "The Nimbus 6 User's Guide."

NASA, Goddard Space Flight Center, Greenbelt, Maryland, 1976. "The Nimbus 6 Catalogs,"Vol. 1, 2.

Paris, J.F., May, 1971. "Transfer of Thermal Microwave in the Atmosphere." Vols. 1, 2. Department of Meteorology, Texas A&M University. Prepared for NASA NGR-44-001-098, Office of Naval Research, Nour 2119 (04), and DOD Project No. 5013, May, 1971.

Sabatini, R.R., May, 1974. "The Application of the Nimbus 5 ESMR to Sea-Surface Wind Determination." EPRF Technical Report 5-74 (ESC) Contract No. N66314-73-C-1572. Prepared by Earth Satellite Corporation.

Sabatini, R.R., February, 1975. "Sea-Surface Wind Speed Estimates from the Nimbus 5 ESMR." EPRF Technical Report 3-75 (ESC) Contract No. N66856-4120-5501. Prepared by Earth Satellite Corporation.

Stogryn, A., July, 1972. "A Study of Radiometric Emission from a Rough Sea-Surface." NASA Contractor Report, NASA CR-2088.

Webster, W.J. Jr., Wilheit, T.T., Ross, D.B., and Per Gloersen, May, 1974. "Analysis of the Convair-990 Passive Microwave Observations of the Sea States During the Bering Sea Experiment." Paper No. 6 in "Results of the U.S. Contribution to the Joint U.S./USSR Bering Sea Experiment," NASA/GSFC Document X-910-74-141, Greenbelt, Maryland.

Wilheit, T.T., Fowler, M.G., Stombach, G., and Per Gloersen, May, 1974. "Microwave Radiometric Determination of Atmospheric Parameters During the Bering Sea Experiment." Paper No. 5 in Results of the U.S. Contribution to the Joint U.S./USSR Bering Sea Experiment," NASA/GSFC Document X-910-74-141, Greenbelt, Maryland.

Wilheit, T.T., and A. Chang, May, 1976. Personal communications.

APPENDIX

EQUATIONS FOR BRIGHTNESS TEMPERATURE CALCULATIONS AND DESCRIPTION OF MODEL ATMOSPHERES

A.1 The Transfer Equation for Microwave - The Thin Atmosphere Approximation

The microwave brightness temperature T_B measured by a radiometer on a satellite may be expressed as:

$$T_B = T(A) + T(S) + T(R) \qquad (1)$$

where T(A) represents the upward emission from the atmosphere, T(S) is the attenuated surface emission, T(R) is the attenuated portion of the reflected downward emission, T(D). These four terms may be expressed as:

$$T(A) = \int_o^\infty T(z)\ \alpha(z) \exp\left(- \int_o^z \alpha(z)\ dz\right) dz$$

$$T(S) = \varepsilon_s T_s \exp\left(- \int_o^\infty \alpha(z) dz\right)$$

$$T(R) = (1 - \varepsilon_s) \exp\left(- \int_o^\infty \alpha(z) dz\right) T(D)$$

and $$T(D) = \int_o^\infty (T)z\ \alpha\ (z) \exp\left(- \int_o^\infty \alpha(z) dz\right) dz$$

In the above equations ε_s and T_s are surface emissivity and temperature, T(z) and $\alpha(z)$ are atmospheric temperature and absorption coefficient as a function of height, z.

The terms of equation (1) can be evaluated numerically by dividing the atmosphere into a finite number of layers of thickness Δz, each with an average temperature and absorption coefficient. For our calculation we used a ten-layer model.

A.2 Absorption Coefficients

Water in all its forms and molecular oxygen are the main absorbers of microwave radiation in the atmosphere. The microwave absorption coefficient of a layer is the sum total of the absorption coefficients of the constituents:

$$\alpha = \alpha_w + \alpha_l + \alpha_i + \alpha_r + \alpha_m + \alpha_o$$

where α_o is the absorption coefficient of molecular oxygen and α_w, α_l, α_i, α_r are the absorption coefficients of water in vapor, small liquid drops, ice, and rain forms; α_m is the absorption coefficient of small melting ice spheres. By "small" are intended cloud particles with an average radius smaller than 50 microns for which the Rayleigh absorption coefficient does not apply. The Rayleigh approximation does not apply to the larger particles constituting rainfall. The absorption coefficient of rain has to be calculated by means of the complex Mie theory.

A.2.1 Absorption Coefficient of Water Vapor

The water vapor absorption is calculated by equations given by Westwater [1, 2]. These equations are:

$$\alpha_w/\rho = (318/T)^{2.5} \exp(-644/T + 644/318)\tilde{\nu}^2 C_1 \{L/[(\tilde{\nu} - \tilde{\nu}_o)^2 + L^2)] + L/[(\tilde{\nu} + \tilde{\nu}_o)^2 + L^2)]\} + (318/T)C_2^o\tilde{\nu}^2 L$$

where α_w = water vapor absorption (km^{-1}),
ρ = water vapor density (gm^{-3})
$L = (\Delta\nu/C_1)w$ = line width (cm^{-1})
$(\tilde{\nu}, \nu_o)$ = wave number and resonant wave number (cm^{-1})
T = absolute temperature (K)

The pressure, P(mb) and temperature dependences of the line width are expressed by:

$$L = (P/1013.25)(318/T)^{.625} a(1 + b\rho)$$

Numerical values of the constants are:

C
$C_1 = .0008312$
$C_2 = .01402$
a = .08478
b = .00708
$\tilde{\nu}_o = .7417\ cm^{-1}$

A.2.2 Absorption Coefficient of Non-Precipitating Clouds

The absorption (or extinction) coefficient for drop size distributions typical of non-precipitating clouds can be expressed in terms of the liquid water content of the cloud particles as shown by Deirmendjian [3]. For wavelengths much larger than the average drop size in a cloud, scattering is negligible and the attenuation can be approximated by Rayleigh's theory. The Rayleigh model of absorption is applicable to clouds whose droplets range from a few microns to a few hundred microns and the absorption coefficient is given by:

$$\alpha = 1.885Q/\lambda\ I\{-K\} \qquad (2)$$

where α = absorption coefficient (km^{-1})
λ = wavelength (cm)
Q = liquid water content (g/m^3)
and $K = (\epsilon - 1)/(\epsilon + 2)$ (3)

where ϵ = complex dielectric constant. The notation I{-K} means the negative of the imaginary part of the complex variable K.

The dielectric constant of water is given as a function of wavelength and temperature T(°K), by Grant, et al. [4] as:

$$\varepsilon = \varepsilon_\infty + (\varepsilon_o - \varepsilon_\infty)/[1 + (i\lambda_s/\lambda)^\beta] \qquad (4)$$

where $\varepsilon_\infty = 4.5$
$\varepsilon_o = 32155.45/T - 29.62$
$\log\lambda_s = 921.0935/T - 2.9014$
$\beta = 0.98$
$i = \sqrt{-1}$

Solving for the imaginary part of K by introducing (4) into equation (3) and using the identity:

$$i = \exp(i\pi/2) = \cos \pi/2 + i \sin \pi/2$$

we obtain for water particles:

$$I\{-K\} = 3\varepsilon_o A^\beta \sin(\pi\beta/2)/D$$

and $A = \lambda_s/\lambda$

$$D = \varepsilon_o + (\varepsilon_\infty + 2)^2(1 + A^{2\beta}) + 2(\varepsilon_\infty + 2)^2 A^\beta \cos(\pi\beta/2) + 2\varepsilon_o(\varepsilon_\infty + 2)[1 + A^\beta \cos(\pi\beta/2)]$$

The dielectric constant of ice is given by Deirmendjian [3] as:

$$\varepsilon = 3.1684 - .008544i$$

and therefore,

$$I\{-K\} = .0009595$$

and,

$$\alpha_i = .0023 \text{ km}^{-1} \text{ at } 37 \text{ GHz}$$

For small drops made of ice and water, K is given by Van de Hulst [5], as:

$$K(\varepsilon_1, \varepsilon_2, q) = \frac{(\varepsilon_2 - 1)(\varepsilon_1 + 2\varepsilon_2) + q^3(2\varepsilon_2 + 1)(\varepsilon_1 - \varepsilon_2)}{(\varepsilon_2 + 2)(\varepsilon_1 + 2\varepsilon_2) + q^3(2\varepsilon_2 - 2)(\varepsilon_1 - \varepsilon_2)}$$

where

ε_1 = inner dielectric constant
ε_2 = outer dielectric constant
q = ratio of inner to total radius

A.2.3 Absorption Coefficient of Rain

When the particle size approaches the wavelength of the incident radiation scattering is appreciable and must be considered along with the absorption, and therefore the attenuation cannot be approximated by the Rayleigh theory. The more complicated Mie model of absorption and scattering must be used. Paris [6] used the Mie theory to calculate the volume absorption coefficient of a polydispersive cloud of hydrometeors obeying the Marshall-Palmer drop-size distribution [7]. The Marshall-Palmer drop-size distribution is fairly representative of the drop-size distribution found in most sub-tropical clouds and can be readily expressed in a rate of precipitation (R, mm/hr) or a liquid water content (M, g/m^3) by the relationship $M = 0.89R^{0.84}$. Paris fitted his results to a regression equation of the form:

$$\alpha_r = kM^d$$

where the absorption coefficient of rain α_r (m^{-1}) is for a Marshall-Palmer raindrop distribution, M is the content of liquid water (gm^{-3}) and k and d are constants which are a function of temperature, T(C). At 37 GHz these are [6]:

$$k = 0.74322 \times 10^{-3} - 0.33730 \times 10^{-5}T + 0.60416 \times 10^{-7}T^2 - 0.35503 \times 10^{-9}T^3 + 0.63349 \times 10^{-11}T^4$$

$$d = 1.0318 - 0.54367 \times 10^{-3}T - 0.19236 \times 10^{-4}T^2 - 0.66322 \times 10^{-6}T^3 + 0.22333 \times 10^{-7}T^4$$

A.2.4 Absorption Coefficient of Molecular Oxygen

The absorption coefficient for molecular oxygen α_o (m^{-1}) is calculated by equations given by Meeks and Lilley [8]. In meteorological units:

$$\alpha_o = 4.6182 \times 10^{-13} (p\,\nu^2/T^3) \cdot \sum_{\substack{N=1 \\ \text{odd}}}^{45} S_N \exp[-2.06844\, N\,(N+1)/T],$$

where

$$S_N = F_o \frac{2(N^2 + N + L)(2N + 1)}{N(N+1)} + F_{N+} \frac{N(2N + 3)}{N + 1} + F_{N-} \frac{(N + 1)(2N - 1)}{N}$$

p is the atmospheric pressure in mb, T is atmospheric temperature in °K, and ν is frequency of radiation in Hz.

F_o, $F_{N\pm}$ are pressure broadening effects which are of the following forms:

$$F_o = \Delta_o/(\nu^2 + \Delta_o^2),$$

and

$$F_{N\pm} = \frac{\Delta_o}{(\nu_{N\pm} - \nu)^2 + \Delta_o^2} + \frac{\Delta_o}{(\nu_{N\pm} + \nu)^2 + \Delta_o^2}$$

$\nu_{N\pm}$ (N = 1, 3, 5, ..., 45) are the resonant frequencies (Hz) for molecular oxygen listed in Table A-1, ν is the frequcncy (Hz) of the radiation under consideration, and Δ_o is the line-width parameter (Hz) for molecular oxygen given by Meeks and Lilley as follows:

$$\Delta_o = 1.4625 \times 10^6 \, p \, (300/T)^{0.85} \, (0.21 + 0.78 \, f)$$

where p is the atmospheric pressure (mb), T is the atmospheric temperature (K), and f is a factor that expresses the relative effectiveness of nitrogen-oxygen collisions as compared to oxygen-oxygen collisions in producing broadening. The value of f changes from 0.75 for very low pressure to 0.25 for high pressures. Meeks and Lilley (1963) give the following empirically-derived form for f:

$$f = \begin{cases} 0.25: & p \geq 356 \text{ mb} \\ 0.25 + 0.435\,(2.551 - \log_{10} p): & 25.3 < p < 356 \text{ mb} \\ 0.75: & p \leq 25.3 \text{ mb} \end{cases}$$

We now have the complete set of equations required to calculate the brightness temperature through the atmosphere by the thin-atmosphere method.

A.3 Atmospheric Models

The atmospheric models used for our brightness temperature calculations are divided into 10 layers from the surface to 15 Km. The layers are, starting from the surface: 1,1,1,1,1,1,2,2,2,3 Km thick, each characterized by an average temperature, pressure, and water vapor. Three types of atmospheres were used as the basis for deriving regres-

sion equations for T_B. These are (1) the U.S. standard atmosphere (1962), (2) a sub-arctic summer atmosphere, and (3) a midlatitude summer atmosphere. All three model atmosphere were taken from Valley [9]. Clouds were inserted only in the U.S. standard atmosphere from one Km to near the freezing level.

To obtain more atmospheric models, the vapor and cloud contents were varied from approximately 50% to 200% higher than the values shown in Tables A-2 to A-4. Atmospheric temperatures remained constant. Calculations were performed for sea-surface emissivities varying from 0.30 to 0.80 and sea-surface temperatures varying from 273°K to 300°K.

TABLE A-1

Resonant frequencies for the absorption of microwaves by molecular oxygen (after Meeks and Lilley, 1963)

N	ν_{N+} (GHz)	ν_{N-} (GHz)	N	ν_{N+} (GHz)	ν_{N-} (GHz)
1	56.2648	118.7505	25	65.7626	53.5960
3	58.4466	62.4863	27	66.2978	53.0695
5	59.5910	60.3061	29	66.8313	52.5458
7	60.4348	59.1642	31	67.3627	52.0259
9	61.1506	58.3239	33	67.8923	51.5091
11	61.8002	57.6125	35	68.4205	50.9949
13	62.4112	56.9682	37	68.9478	50.4830
15	62.9980	56.3634	39	69.4741	49.9730
17	63.5685	55.7839	41	70.0000	49.4648
19	64.1272	55.2214	43	70.5249	48.9582
21	64.8779	54.6728	45	71.0497	48.4530
23	65.2240	54.1294			

TABLE A-2

U.S. STANDARD ATMOSPHERE FOR T_B CALCULATIONS

Layer	Approx. Height (km)	Pressure (mb)	Temp. (°K)	Water Vapor (gm^{-3})	Cloud Liquid Water (gm^{-3})
1	0.5	956	285	10.56	
2	1.5	847	278	6.73	0.2
3	2.5	748	272	4.48	0.2
4	3.5	659	265	2.15	
5	4.5	579	259	1.33	
6	5.5	506	252	0.95	
7	7.0	411	243	0.37	
8	9.0	308	230	.80	
9	11.0	227	217	.01	
10	13.5	154	217	.00	
Total Precipitable Water (cm)				2.71	0.04

TABLE A-3

MIDLATITUDE SUMMER ATMOSPHERE FOR T_B CALCULATIONS

Layer	Approx. Height (Km)	Pressure (mb)	Temp. (°K)	Water Vapor (gm^{-3})
1	0.5	958	289	13.51
2	1.5	852	285	10.56
3	2.5	756	280	7.68
4	3.5	669	275	5.50
5	4.5	591	269	3.62
6	5.5	521	261	0.80
7	7.0	426	248	0.40
8	9.0	324	232	0.10
9	11.0	243	217	0.02
10	13.5	166	217	0.00
Total Precipitable Water (cm)				4.27

TABLE A-4

SUBARCTIC SUMMER ATMOSPHERE FOR T_B CALCULATIONS

Layer	Approx. Height (km)	Pressure (mb)	Temp. (°K)	Water Vapor (gm^{-3})
1	0.5	958	285	7.50
2	1.5	845	279	5.10
3	2.5	747	274	3.45
4	3.5	658	269	2.20
5	4.5	579	263	1.35
6	5.5	507	257	0.77
7	7.0	413	246	0.28
8	9.0	311	232	0.02
9	11.0	230	225	0.01
10	13.5	158	225	0.00
Total Precipitable Water (cm)				2.10

REFERENCES

[1] Westwater, E.R., "An Analysis of the Correction of Range Errors Due to Atmospheric Refraction by Microwave Radiometric Techniques," ESSA Technical Report IER 37-ITSA 37, 1967.

[2] Westwater, E.R., "Microwave Emission from Clouds," NOAA Technical Report ERL 219-WPL 18, 1972.

[3] Deirmendjian, D., "Complete Microwave Scattering and Extinction Properties of Polydispersed Cloud and Rain Elements," Rand Corp. Report R-422-PR, USAF Contract No. AF-49 (638)-700, 1963.

[4] Grant, E.H., T.J. Buchanan, and H.F. Cook, "Dielectric Behavior of Water at Microwave Frequencies," J. Chem. Phys. Vol. 26, pp. 156-161, 1957.

[5] Van de Hulst, H.C., "Light Scattering by Small Particles," Wiley and Co., New York, N.Y., 1957.

[6] Paris, J.F., "Transfer of Thermal Microwave in the Atmosphere," Vols. 1, 2, Dept. of Meteor. Texas A&M University, 1971.

[7] Marshall, J.S. and W. McK. Palmer, "The Distribution of Raindrops with Size," J. Meteor. Vol. 5, pp. 165-155, 1948.

[8] Meeks, M.L., and A.E. Lilley, "The Microwave Spectrum of Oxygen in the Earth's Atmosphere," J. Geophys, Res., 68, 1683-1703, 1963.

[9] Valley, S.L. (ed), "Handbook of Geophysics and Space Environments," Air Force Cambridge Research Laboratories, USAF, 1965.